2011

A Multifaceted Phenomenon of Hydrophobic Effects: Insights Learned from Nucleation Algorithm Based Computer Simulation Approach

Hyunmi Kim
Louisiana State University and Agricultural and Mechanical College

A MULTIFACETED PHENOMENON OF HYDROPHOBIC EFFECTS: INSIGHTS LEARNED FROM NUCLEATION ALGORITHM BASED COMPUTER SIMULATION APPROACH

A Dissertation
Submitted to the Graduate Faculty of the
Louisiana State University and
Agricultural and Mechanical College
in partial fulfillment of the
requirements for the degree of
Doctor of Philosophy

in

The Department of Chemistry

by
Hyunmi Kim
B.S., Chung-Ang University, Korea, 2002
M.S., Seoul National University, Korea, 2004
December, 2011

To

Euiyong Hwang and Brian K Hwang,

ACKNOWLEDGEMENTS

I am deeply grateful to my advisor, Professor Bin Chen, for whom I have the utmost respect. During my doctoral program in the Chemistry Department at Louisiana State University, I owe him many things from academic to personal (or human) aspects. Especially, I appreciate his generous support when my family suffered difficulties in 2008 when my son Brian was born.

I am also sincerely grateful to Professor Evqueni E. Nesterov. He served on my committee and was the advisor of my husband, Euiyong Hwang, who was also a graduate student in the Chemistry Department at Louisiana State University. He always showed concern for my family and gave us encouragement and support whenever our family had difficulties.

I deeply appreciate the effort of my advisory committee members: Professor Randall Hall, Professor Erwin Poliakoff, and Professor Chunyan Li. I also would like to thank my laboratory group members, Matt Mckenzie, Ricky Nella, and Samuel Keasler. They all have good personalities and were always willing to help me and each other. I was so lucky to have such a good group of members.

To my friends, Dr. Jungyoung Cho, Dr. Gyun-Tack Bae, Dr. Wonbae Lee, Dr. Jeonghoon Lee, Chang-uk Lee, Dr. Jinwoo Choi, Sang Gil Youm, Sung-Gun Park, and Dr. Hana Kim, I really thank you for all your great help and advice with regard to living as a graduate student away from home. I would like to express special thanks to Sang Gil Youm and Hana Kim. Sang Gil and Hana are like my family, and I owe many things to them. I am also thankful to Dr. Michelle Thiaville for valuable advice and comments on my dissertation.

With all of my love, I would like to show my appreciation to my husband, Euiyong Hwang, and my son, Brian K Hwang. My two greatest fortunes are the fact that I met my husband and I gave birth to my son, Brian K Hwang. They are my life and I always appreciate that they are my

family. I really hope that my family loves each other forever and are healthy. I also hope that my son, Brian, grows up healthy and to be a wise person. Finally, I am sincerely grateful to my parents, my sisters, and my parents-in-law for supporting and encouraging me to continue and finish my doctoral program.

Without all their support, I could not be finishing this step of my doctoral program. I am deeply grateful to all again. Thank you so much !!! And I love you all.

TABLE OF CONTENTS

LIST OF TABLES

LIST OF FIGURES

ABBREVIATIONS

ABH	- Association barrier height
AVBMC	- Aggregation volume bias Monte Carlo
AVUS-HR	- Aggregation volume bias Monte Carlo combined with umbrella sampling and histogram reweighting
BH	- Barrier height
CM	- Contact minimum
CNT	- Carbon nanotube
DBH	- Dissociation barrier height
FDM	- Finite difference method
HR	- Histogram reweighting
MC	- Monte Carlo
MCM-48	- Mobil composition of matter No. 48
MD	- Molecular dynamics
MW	- Molecular weight
NFE	- Nucleation free energy
NPT	- A system with a fixed number of atoms N, pressure P, and temperature T
NVT	- A system with a fixed number of atoms N, volume V, and temperature T
PEG 20K	- Polyethylene glycol with molecular weight of 20000
PMF	- Potential of mean force
Rd-apocyt B562	- Octadecyltrichlorosilane
RNase A	- Ribonuclease A
SPC	- Simple point charge
SSM	- Solvent separated minimum
ST2	- A water model proposed by Stillinger and Rahman
TIP3P	- Transferable intermolecular potential with 3 Points
TIP4P	- Transferable intermolecular potential with 4 Points
US	- Umbrella sampling

ABSTRACT

We have applied our new approach, a combination of the AVUS-HR nucleation algorithm and a thermodynamic cycle, to the studies of hydrophobicity-related researches. Due to the multifaceted characteristics of hydrophobicity, it is essential to acquire knowledge in various environments where hydrophobic relevant events occur for comprehensive understanding of this process. In this regards, we have chosen two relatively unstudied hydrophobic subjects for application of our new methodology.

For the first subject, hydrophobic association behaviors of a methane pair confined into a nanometer sized hydrophobic cavity have been investigated. Our new approach demonstrates that the association behavior between two methane molecules is enhanced under confined environment rather than in bulk water. This association is primarily driven by energy originating from the unique situation where small (i.e., two methane molecules) and large (i.e., boundary of the hydrophobic cavity) hydrophobic units come together.

For the second subject, hydration thermodynamics for confined spaces between two infinitely parallel walls have been studied. Our simulation results demonstrate that the weak attractive interaction between water molecules and walls allows water molecules to pack more efficiently for the smallest wall separation of 3 Å considered here comparing with the hard wall case where there is no interaction between water molecules and walls. Furthermore, these weak attractive interactions lower the free energy penalty for the formation of water clusters inside a confined space, ultimately lowering the total energy of the system when compared with the hard wall.

Based on the successful applications of our novel nucleation algorithm to the two different hydrophobic related researches, further, we believe that it will contribute to the various and more complex hydrophobic researches (i.e., association behaviors of nonpolar and/or polar amino acid residues in the presence of salts under confined environment, and effects of salts, temperature

and pressure on this association behaviors) as well as nucleation studies under confined environment.

CHAPTER 1 INTRODUCTION.

1.1 Overview of Hydrophobicity.

Although extensive research in the area of hydrophobicity has previously been performed, it is still a central research topic due to its pivotal role in many areas such as biology, geology, and technology. For example, it is believed that water induced hydrophobic interaction is one of the major contributing factors for many biological self-assembly processes such as the formation of micelles and/or biological membranes, and protein folding.[1, 2] Given that these types of hydrophobic interactions are difficult to study in vitro and in vivo, new research techniques are being continually employed to further characterize these interactions.

Despite the widely used concept of hydrophobicity, however, there are continued debates about the meaning of it.[3-5] Blokziji and Engberts stated that "Many of the existing definitions of hydrophobic effects reflect the lack of clarity with respect to the exact meaning of the terms that have been introduced to describe the unusual thermodynamic behavior of apolar solutes in aqueous solution." in their review paper, "Hydrophobic Effects. Opinions and Facts".[5] During his discussions in *Science*,[3] Dill stated that the most sensible use of hydrophobicity is the situation where "it has been used more specifically to refer to transfer of nonpolar solutes into aqueous solutions when a particular characteristic temperature dependence is observed.". This definition appears to be most used one among many existing definitions of it, and is also simply based on the experimental observation of unusual features of nonpolar solvation in water, where nonpolar solvation in aqueous solution is strongly controlled by unfavorable entropy at around room temperature with a large positive heat capacity change while that in non-aqueous solution is principally controlled by enthalpy over a broad range of temperatures with small heat capacity change, as first identified by Butler and Reid[6] and later by Frank and Evans[7].[3,5]

Frank and Evans,[7] the first scientists to attempt to explain the molecular origins of this unusual features of nonpolar solvations in water, have proposed the "iceberg model" - the first classical model for hydrophobic effects. This model states, "When a rare gas atom or non-polar molecule dissolves in water at room temperature it modifies the water structure in the direction of greater "crystallinity"-the water, so to speak, builds a microscopic iceberg around it".[7] So they have attributed the loss of entropy for the solvation of nonpolar molecules in water at around room temperature to the production of "freezing" of water near nonpolar molecules and large heat capacity change for the elevation of temperature to melting of this iceberg.

On the other hand, a classical hydrophobic interaction model originated from Kauzmann's entropy origin of hydrophobic attraction model. In his influential 1959 paper,[8] Kauzmann suggested that the way protein's composite amino acid chains fold into buried hydrophobic residues and exposed hydrophilic ones in an aqueous environment is analogous to micelle formation of amphilphic molecules such as detergent in an aqueous solution. He referred to this tendency of non-polar groups of proteins to adhere to one another in aqueous environments as "hydrophobic bonding". He was also the first to suggest, based on his observations, that this hydrophobic bonding (or hydrophobic interaction) plays a major role in stabilizing the folded states of native proteins which is qualitatively similar to the requirements for the transfer of a hydrophobic solute from its pure phase into water.

Another researcher, Ben-Naim,[9, 10] who performed pioneering work in hydrophobic interaction area, has used classical statistical mechanics to produce a theoretical model for demonstrating the tendency of two nonpolar molecules to adhere to each other in aqueous environments. They defined "hydrophobic interaction process" as the process of bringing two solutes from a fixed position at infinite separation (he noted in his book of "Hydrophobic interaction", that infinite separations actually means large enough separation where there is no

correlation between the positions of the two solutes.) to some distance, *R*, separation and expressed the Gibbs free energy change ($\Delta G(R)$) corresponding to this process as follows:

$$\Delta G(R) = U_{SS}(R) + \delta G^{HI}(R)$$

Where $U_{SS}(R)$ is the direct pair potential between solute molecules which is not dependent on the properties of solvent molecules, and $\delta G^{HI}(R)$ is an indirect part arising from the presence of solvent molecules. Sometimes, a second term, $\delta G^{HI}(R)$, is used as a measurement of hydrophobic interactions. From the Gibbs free energy definition, the force exerted between two particles, $F_{ss}(R)$, can be written as follows:

$$F_{SS}(R) = -\frac{\partial \Delta G(R)}{\partial R}$$

From the above equation, when the value of $F_{ss}(R)$ is negative, the force operating between two solute molecules is attractive, thus the force is repulsive when $F_{ss}(R)$ is positive.

The resulting value is the potential of mean force (PMF) between two solute pairs, $\Delta G(R)$, and can be obtained from their pair distribution functions in aqueous solution by as followed equation:

$$g_{SS}(R) = \exp[-\Delta G(R)/k_B T]$$

$$= \exp[-U_{SS}(R)/k_B T] \times \exp[-\delta G^{HI}(R)/k_B T]$$

Where $g_{SS}(R)$ is the pair distribution function providing the probability of finding a second solute molecule S at a distance R from the center of reference particle S and $k_B T$ is Boltzmann factor times temperature.

Due to the difficulties of experimentally measuring the indirect part of the solvent induced interactions, $\delta G^{HI}(R)$, computer simulation studies are recognized as a valuable source for understanding the solvent mediated interactions between nonpolar solute molecules. Many simulation studies[11-21] have been successful at identifying the molecular origin of hydrophobic

interactions between two small nonpolar molecules in infinitely dilute aqueous solutions. For example, PMFs for a pair of simple small nonpolar solute such as methane as a function of their separation distance R, and its dependence on temperature,[11-14] pressure,[15] and water solvent models[22] have been well studied.

Due to the multifaceted nature of hydrophobic interactions, a comprehensive understanding of the function of hydrophobic interactions has not been clear enough although behaviors of small nonpolar solute molecule in infinitely dilute aqueous solution has been well established. Understanding of the behaviors of small hydrophobic molecules in dilute aqueous solution is to see just one side of pictures of hydrophobicity. In order to provide broader insight into the mechanisms of these interactions in different environments where hydrophobic relevant events occur, various situations need to be considered. In the following, we have provided a brief description of hydrophobicity in two different environments that are relatively less focused.

One of the environments where hydrophobic relevant event occur is the confinement. It was previously reported that confined environments can significantly alter the water structure, which is essential for the existence of hydrophobic interactions, producing phase behavior quite distinct from bulk water and/or water clusters not under confinement.[23, 24] In addition, these alterations to the water structure can significantly modify its interactions with solute molecules. For example, in a solvent driven process such as protein folding, perturbing the solvent structure by confinement can produce considerably different protein structures than those observed in bulk phases. In particular this confinement is considered to be one of the most important factors required for understanding the behavior of biological molecules in the cellular environment.

The cellular environments where biomolecules function is complex, crowded, and different from the infinitely dilute idealized one where most theoretical, experimental, and computational studies for the predictions of interaction behavior of these molecules is performed.[25-29] The

importance of both environmental confinement and macromolecular crowding are two potential factors that are necessary for creating a complex cellular environment.[25-28] These two factors are related, but distinct from each other based upon the origin for excluded volume:[29] Confinement is used when referring to the excluded volume effects by a boundary of confined space to a substance of interest. Conversely, macromolecular crowding is used when referring to the exclusion of volumes to a substance of interest by the presence of other macromolecules.

Recent published studies[30-33] have reported that both confinement and crowding affect the protein behaviors such as equilibrium, kinetics of protein folding, and protein-protein binding abilities. Although both factors influence the stability of proteins, it has been reported that confinement has a significant effect on protein stability while crowding has only a modest effect on it. This difference has been noted consistently by experimental studies from both different laboratories[30-32] and theoretical works.[33] For instance, the stability of the protein ribonuclease A(RNase A) is drastically increased ($\Delta T_m \cong 30$ C) by encapsulation in the mesoporous silicate system MCM-48.[31] On the other hand, Ai et al[32] reported that the stability of the mutant protein of a redesigned apocytochrome B562 increases by ≅ 0.25 kcal/mol in the presence of 85 g/L PEG 20K (MW ≅ 20000) when compared with the absence of crowding agent.

Several experimental studies have demonstrated that the stability of the folded/unfolded state and the folding rate for biological molecules, such as protein, observed under confinement is different from those observed in bulk water. One important finding from these studies is that the relative stability of the folded state to the unfolded one is enhanced under confinement compared to bulk water.

Another obstacle for generalizing (or quantifying) the hydrophobic interactions in one simple term is the “length scale” dependence of these interactions. This dependency is a characteristic difference derived from whether small hydrophobic units (or a small apolar group in dilute

aqueous solution) or large hydrophobic ones (or a relatively high concentrations of apolar groups and/or large aggregation or assemblies of them in aqueous solutions) are involved in the interaction. It has been generally accepted[34] that water molecules can simply maneuver around small hydrophobic molecules (0.2 nm ~ 0.5 nm), with most of them each participating in four hydrogen bonds like pure liquid water. In this case, the free energy cost for solvating water molecules is entropy relevant because merely reordering a network of hydrogen bonding near hydrophobic units does not require physical breakage of these bonds.

The previous example, however, isn't applicable to water molecules in a geometrical network of hydrogen bonding near large hydrophobic units. In this case, one water molecule has less than four hydrogen bondings which results in energetic driven solvation free energy. Some theoretical works have shown that this resulting energetic cost induces drying near the surface of hydrophobic units producing liquid–vapor like interfaces, which is a significant difference from small hydrophobic units. For example, Chandler[34] has shown the existence of wetting and/or dewetting behaviors for a series of ideal hydrophobic solute models of different sizes with a radius from 0.4 to 100 nm by calculating the density of solvent relative to that of the bulk solvent near them. When the radius equals 0.4 nm, the smallest cavity considered in this study, water density is immediately increased by a factor of about two adjacent to this cavity thus defining the interaction as - "wet". In contrast, for larger cavities with radii of 1, 10, or 100 nm, an appreciable amount of water depletion has been detected near the surface leading to their characterization as "dewetted" or "dry".

Computer simulation studies have also modeled this dewetted phenomenon for large hydrophobic units in water. Early computer simulation studies[35-37] have shown depletion of water was not observed near extended hydrophobic surfaces. For instance, these studies observed no water depletion that could be attributed to an absence of large density fluctuations produced

near extended hydrophobic surface drying.[38] Wallqvist and Berne[39] calculated the potential of mean force between two large parallel hydrophobic oblate ellipsoidal plates in liquid water based on thermodynamic perturbation theory and constant–pressure molecular dynamics. In contrast to earlier studies,[35-37] they have observed a dewetting transition when the plates are moved close enough together that two water layers cannot fit between them. This observation is significant because one layer of water is never observed even though the distance between the two plates can accommodate it. Interestingly, however, Hummer and colleagues[40] have shown that water molecules can enter a narrow hydrophobic pore, such as carbon nanotubes (CNT), which can also only accommodate one layer of water molecules. Considering both the loss of hydrogen bonding when water molecules enter a hydrophobic CNT with a narrow hollow, and the weak attractive interaction parameters between water and the CNTs, it is surprising that hydration of the interior of nanotube with a one dimensional system of water molecules was observed. The researchers attributed such hydration of narrow and hydrophobic interiors of CNTs to the water binding energy distribution. In contrast to properties of bulk water, where there is broader distribution of both low energy and high energy states, water binding energies inside the nanotube are more sharply and strongly distributed around moderate energy thus providing a lower excess chemical potential compared to bulk water. This difference results in a favorable excess chemical potential that functions as a driving force for water to enter inside the CNT. The researchers[40] also suggested that it may be possible to control wet-dry transitions by producing small alterations in properties such as the interaction potential between the water molecules and CNTs though this remains to be tested.

Another question arising from the length scale dependence of hydrophobicity is “When do crossover behaviors occur between small and large hydrophobic solute hydration?” Some

theoretical studies[34, 41] have reported that crossover behavior between two regimes occurs at nanometer length scales.

With finishing Chapter 1 in my dissertation, the purpose of this dissertation is to address two aspects of hydrophobic interactions that have been relatively ignored in order to provide further insight into the mechanisms of these interactions in different environments where hydrophobic relevant events occur: The first aspect my dissertation will focus on is water induced interactions for small hydrophobic molecules in the confined environment and while the second aspect will characterize water induced hydrophobic interaction for large hydrophobic objects. Overall, this dissertation will add to the breadth of knowledge needed for characterizing hydrophobicity in various environmental situations.

1.2 References.

(1) Dill, K. A., Dominant forces in protein folding, *Biochemistry* **1990**, *29*, 7133-7155.

(2) Tanford, C. *The Hydrophobic Effect: Formation of Micelles and Biological Membranes*; John Weiley: New York, 1973.

(3) Dill, K. A.; Privalov, P. L.; Gill, S. J.; Murphy, K. P., The Meaning of Hydrophobicity, *Science* **1990**, *250*, 297-298.

(4) Gill, S. J.; Murphy, K. P., The meaning of hydrophobicity - response, *Science* **1990**, *250*, 298-299.

(5) Blokzijl, W.; Engberts, J. B. F. N., Hydrophobic Effects. Opinions and Facts, *Angew. Chem., Int. Ed.* **1993**, *32*, 1545-1579.

(6) Butler, J. A. V.; Reid, W. S., 249. The solubility of non-electrolytes. Part III. The entropy of hydration, *Journal of the Chemical Society (Resumed)* **1936**, 1171-1173.

(7) Frank, H. S.; Evans, M. W., Free Volume and Entropy in Condensed Systems III. Entropy in Binary Liquid Mixtures; Partial Molal Entropy in Dilute Solutions; Structure and Thermodynamics in Aqueous Electrolytes, *J. Chem. Phys.* **1945**, *13*, 507-532.

(8) Kauzmann, W., Some factors in the interpretation of protein denaturation, *Adv. Protein Chem.* **1959**, *14*, 1-63.

(9) Ben-Naim, A. *Water and Aqueous Solutions*; Plenum: New York, 1974.

(10) Ben-Naim, A. *Hydrophobic Interactions*; Plenum: New York, 1980.

(11) Chan, H. S., temperature dependence hydrophobic interactions: mean force perspective, effects water density, nonadditivity thermodynamic signatures, *J. Chem. Phys.* **2000**, *113*, 4683-4700.

(12) Lüdemann, S.; Schreiber, H.; Abseher, R.; Steinhauser, O., The influence of temperature on pairwise hydrophobic interactions of methane-like particles: A molecular dynamics study of free energy, *J. Chem. Phys.* **1996**, *104*, 286.

(13) Paschek, D., Temperature dependence of the hydrophobic hydration and interaction of simple solutes: an examination of five popular water models, *J. Chem. Phys.* **2004**, *120*, 6674-6690.

(14) Shimizu, S.; Sun Chan, H.; Chan, H. S.; Hue Sun, C., Temperature dependence of hydrophobic interactions: A mean force perspective, effects of water density, and nonadditivity of thermodynamic signatures, *J. Chem. Phys.* **2000**, *113*, 4683-4700.

(15) Ghosh, T.; García, A. E.; Garde, S., Molecular dynamics simulations of pressure effects on hydrophobic interactions, *J. Am. Chem. Soc.* **2001**, *123*, 10997-11003.

(16) Berne, B. J., free energy hydrophobic interaction from molecular dynamics simulations:a effects solute solvent polarizability, *J. Phys. Chem. B* **1997**, *101*, 10488-10493.

(17) Smith, D. E.; Haymet, A. D. J.; David E. Smith, A. D. J. H., Free energy, entropy, and internal energy of hydrophobic interactions: Computer simulations, *J. Chem. Phys.* **1993**, *98*, 6445-6454.

(18) Sobolewski, E.; Makowski, M.; Czaplewski, C.; Liwo, A.; Ołdziej, S.; Scheraga, H. A., Potential of mean force of hydrophobic association: dependence on solute size, *J. Phys. Chem. B* **2007**, *111*, 10765-10774.

(19) Dang, L. X., Potential of mean force for the methane-methane pair in water, *J. Chem. Phys.* **1994**, *100*, 9032-9034.

(20) Haymet, A. D. J., free energy, entropy, internal energy hydrophobic interactions: computer simulations, *J. Chem. Phys.* **1993**, *98*, 6445-6454.

(21) Li, J.-L.; Car, R.; Tang, C.; Wingreen, N. S., Hydrophobic Interaction and Hydrogen-Bond Network for a Methane Pair in Liquid Water, *Proc. Natl. Acad. Sci. USA* **2007**, *104*, 2626-2630.

(22) Van Belle, D.; Wodak, S. J., Molecular dynamics study of methane hydration and methane association in a polarizable water phase, *J. Am. Chem. Soc.* **1993**, *115*, 647-652.

(23) Zangi, R., Water confined to a slab geometry: a review of recent computer simulation studies, *J. Phys.-Condens. Mat.* **2004**, *16*, 0-S5388.

(24) Zangi, R.; Mark, A. E., Monolayer ice, *Phys. Rev. Lett.* **2003**, *91*, 025502.

(25) Ellis, R. J., Macromolecular crowding: obvious but underappreciated, *Trends Biochem. Sci.* **2001**, *26*, 597-604.

(26) Ellis, R. J.; Minton, A. P., Protein aggregation in crowded environments, *Biol. Chem.* **2006**, *387*, 485-497.

(27) Minton, A. P., How can biochemical reactions within cells differ from those in test tubes?, *J. Cell Sci.* **2006**, *119*, 2863-2869.

(28) Minton, A. P., Macromolecular crowding, *Curr. Biol.* **2006**, *16*, R269-R271.

(29) Zhou, H. X.; Rivas, G.; Minton, A. P., Macromolecular crowding and confinement: biochemical, biophysical, and potential physiological consequences, *Annu. Rev. Biophys.* **2008**, *37*, 375-397.

(30) Eggers, D. K.; Valentine, J. S., Molecular confinement influences protein structure and enhances thermal protein stability, *Protein Sci.* **2001**, *10*, 250-261.

(31) Ravindra, R.; Zhao, S.; Gies, H.; Winter, R., Protein encapsulation in mesoporous silicate: the effects of confinement on protein stability, hydration, and volumetric properties, *J. Am. Chem. Soc.* **2004**, *126*, 12224-12225.

(32) Ai, X.; Zhou, Z.; Bai, Y.; Choy, W. Y., 15N NMR spin relaxation dispersion study of the molecular crowding effects on protein folding under native conditions, *J. Am. Chem. Soc.* **2006**, *128*, 3916-3917.

(33) Zhou, H. X., Protein folding in confined and crowded environments, *Arch. Biochem. Biophys.* **2008**, *469*, 76-82.

(34) Chandler, D., Interfaces and the driving force of hydrophobic assembly, *Nature* **2005**, *437*, 640-647.

(35) Lee, C.-Y.; McCammon, J. A.; Rossky, P. J., The structure of liquid water at an extended hydrophobic surface, *J. Chem. Phys.* **1984**, *80*, 4448-4455.

(36) Wallqvist, A.; Berne, B. J., Hydrophobic interaction between a methane molecule and a paraffin wall in liquid water, *Chem. Phys. Lett.* **1988**, *145*, 26-32.

(37) Bratko, D.; Blum, L., monte carlo simulation hydrophobic interaction, *J. Chem. Phys.* **1987**, *86*, 2955-2959.

(38) Lum, K.; Chandler, D.; Weeks, J. D.; Lum, K.; Chandler, D.; Weeks, J. D., Hydrophobicity at Small and Large Length Scales, *J. Chem. Phys. B* **1999**, *103*, 4570-4577.

(39) Wallqvist, A.; Berne, B. J., Computer Simulation of Hydrophobic Hydration Forces on Stacked Plates at Short Range, *J. Phys. Chem.* **1995**, *99*, 2893-2899.

(40) Hummer, G.; Rasaiah, J. C.; Noworyta, J. P., Water conduction through the hydrophobic channel of a carbon nanotube, *Nature* **2001**, *414*, 188-190.

(41) Chandler, D.; Weeks, J. D., hydrophobicity small large length scales, *J. Phys. Chem. B* **1999**, *103*, 4570-4577.

CHAPTER 2 METHODOLOGY.

2.1 Introduction.

All the research in this dissertation was performed based on the AVUS-HR technique originally developed by Chen et al.[1] This technique was originally developed by using a combination of Aggregation Volume Bias Monte Carlo (AVBMC),[2, 3] Umbrella Sampling (US),[4] and Histogram Reweighing (HR)[5, 6] for the purpose of adjusting sampling problems during rare nucleation events in configuration space. In the following sections, a description of the development for AVUS-HR will be discussed first, followed by discussion of the Metropolis algorithm,[7] AVBMC, US, and HR techniques, respectively. Finally, applications of the nucleation algorithm method to hydrophobicity-related research will be discussed.

2.2 AVUS-HR Approach.

2.2.1 Nucleation in Computer Simulations.

Understanding the nucleation process is important in many scientific fields such as nanotechnology, coastal and atmospheric science, and molecular biology. For example, nucleation is the critical first step in forming atmospheric aerosol particles, which directly influence human lives through both their climatic and health effects.[8, 9]

The specific formation of vapor-liquid nucleation is a relaxation process forming the more stable liquid droplets from a metastable mother phase of supersaturated vapor. It is also well known that vapor-liquid nucleation is a thermally activated process characterized by a nucleation free energy barrier at the critical nuclei.

Theoretically, it would be straightforward to perform the MD (Molecular Dynamics) simulation for nucleation event since it allows direct calculation of the average properties of system based on real time evolution of the event.[10] However, there is an extremely low

probability of forming critical nuclei making it difficult to prove and quantify the related thermodynamic properties of this process in the limit of allowed time scale for MD simulation. Alternately, MC (Monte Carlo) simulation can provide useful method by performing specially designed MC moves for liquid droplet formation and destruction.

Metropolis Monte Carlo method would be one of the simplest methods used to calculate the free energy of forming liquid droplets in a supersaturated vapor (shown in Equation 2-1):

$$\Delta G(N) = -k_B T In \frac{P(N)}{P(1)} \qquad 2\text{-}1$$

Where $\Delta G(N)$ is the free energy change of forming an N-mer from N number of monomers, k_B is the Boltzmann constant, T is the temperature, and $P(N)$ and $P(1)$ are the concentrations of the N-mer and the monomer, respectively. Like the limitation of MD simulation, this efficient algorithm is not an appropriate method for the study of nucleation events because the number of Monte Carlo moves required to form a critical cluster would be computationally intractable at any reasonable set of simulation conditions. In this regard, the AVUS-HR algorithm was later developed for an efficient sampling of rare nucleation events.

2.2.2 Metropolis Monte Carlo Method.[7]

In 1953, Metropolis et al.[7] have shown the efficient Monte Carlo sampling algorithm for obtaining the average value of a measurable property, A, depicted in Equation 2-2.

$$< A >= \frac{\int dr^N \exp[-\beta U(r^N)] A(r^N)}{\int dr^N \exp[-\beta U(r^N)]} \qquad 2\text{-}2$$

The main idea of this algorithm is to sample only important points having a non-negligible Boltzmann factor and weight them evenly. This efficient strategy is in contrast to the conventional Monte Carlo scheme of generating all the points with equal probability and weighting them by their Boltzmann factor used for calculating the <A>. The equations below

[(2-3) to (2-5)] from Ref.11 [11] provide a detailed description of this method. Assuming that the points in configuration space can be randomly generated according to $P(r^N)$.

$$P(r^N) = \frac{\exp[-\beta U(r^N)]}{\int dr^N \exp[-\beta U(r^N)]} \qquad 2\text{-}3$$

$$Z_i = LN(r^N) \qquad 2\text{-}4$$

$$< A >= \frac{1}{L} \sum_{i=1}^{L} Z_i A(r_i^N) \qquad 2\text{-}5$$

In Equation 2-3, N is the number of particles, r^N stands for the coordinates of all N particles, and $P(r^N)$ is the probability of the density when finding the system in a configuration around r^N. If we assume that it is able to randomly generate points in configuration space according to $P(r^N)$, the number of points, Z_i generated per unit volume around a point r^N is equal to $LP(r^N)$. Here L is the total number of points generated. So, by applying the information from Equations 2-3 and 2-4, equation 2-2 can be rewritten as Equation 2-5. In other words, the Metropolis method requires only $\exp[-\beta U(r^N)]$, the relative but not the absolute probability of visiting different points in configuration space, for obtaining the $<A>$ value, while direct Monte Carlo needs to calculate both $\exp[-\beta U(r^N)]$ and the configuration part of the partition function (denoted by the Z_i term). Where $\beta = 1/k_BT$ and $U(r^N)$ is the potential energy of the system around r^N.

These efficient Metropolis Monte Carlo moves are accomplished by the following steps:

1) Randomly select particle i having a non-negligible Boltzmann factor $\exp[-\beta U(\text{old})]$, and calculate its energy, E_{old}.

2) Give particle i a small displacement for generating a new configuration and calculate its energy, E_{new}.

3) Calculate the energy difference between old and new configurations, $\Delta E = E_{new} - E_{old}$. In step 3, a decision must be made whether to accept or reject the new (n) configuration based on the

constraint that, on average, the probability of finding the system in a new configuration is proportional to *N*(n). When the move is constructed, the "detailed balance" has to be satisfied. This term attributes that the average number of accepted trial moves from an old state to any new states is equal to the number of reverse moves in equilibrium (as shown in Equation 2-6):

$$N(o)\pi(o \to n) = N(n)\pi(n \to o) \qquad 2\text{-}6$$

In this equation, the transition matrix, $\pi(o \to n)$, can be constructed according to the Monte Carlo moves in order to transform the equation as needed. For example, the probability of performing a trial move from old to new can be expressed as $\alpha(o \to n)$, where α is referred to as the underlying matrix of the Markov chain. The acceptance probability, $acc(o \to n)$, which determines whether to accept or reject this trial move, is the next step in manipulating the Monte Carlo equation:

$$\pi(o \to n) = \alpha(o \to n) \times acc(o \to n) \qquad 2\text{-}7$$

Now, Equation 2-6 can be rewritten by substituting Equation 2-6 into 2-7 to produce Equation 2-8:

$$N(o) \times \alpha(o \to n) \times acc(o \to n) = N(n) \times \alpha(n \to o) \times acc(n \to o) \qquad 2\text{-}8$$

In the original Metropolis scheme, α is chosen to be symmetric, thus, $\alpha(o \to n) = \alpha(n \to o)$. Now equation 2-8 can be rewritten as follows:

$$N(o) \times acc(o \to n) = N(n) \times acc(n \to o) \qquad 2\text{-}9$$

$$\frac{acc(o \to n)}{acc(n \to o)} = \frac{N(n)}{N(o)} = \frac{\exp[-\beta U(n)]}{\exp[-\beta U(o)]} = \exp\{-\beta[U(n) - U(o)]\} \qquad 2\text{-}10$$

Any set of acceptance rates meeting the above criterion will yield the correct equilibrium distribution and Metropolis et al. chose $acc(o \to n) = \min[1, \exp\{-\beta[U(n) - U(o)]\}]$.

These assertions now produced two more Metropolis Monte Carlo steps:

4) Accept the new configuration with a probability min[1,exp{-β[U(n) – U(o)]}.

5) Whether the new configuration is accepted or not, compute the value of A for the new configuration.

The resulting sampling algorithm is more efficient than the conventional Monte Carlo algorithm making it widely used. However, it is clearly neither efficient nor adjustable to sampling nucleation events for strongly association fluids due to the unique sets of problems posed by nucleation events.

2.2.3 The Aggregation-Volume-Bias Monte Carlo Algorithm (AVBMC).[2,3]

One of the major difficulties in using the Metropolis method for the studies of vapor-liquid nucleation events is the extremely inefficient sampling of dynamic hopping events between bonded (liquid cluster) and non-bonded (vapor) configurations for strongly associating fluids. This is because that the probability of performing a trial move that goes from a non-bonded configuration to a bonded one is very low due to a small volume portion of bonded configurations in the vast total volume of phase space, and that acceptance rate for any trial move resulting in the destruction of the bonded configuration once it is found, is very low due to the favorable energy for a bonded one. In order to solve these hopping problems between liquid cluster (bonded) and vapor phase (nonbonded), Aggregation-Volume-Bias Monte Carlo (AVBMC) was developed by introducing a novel trial move called an intrabox swap move. An AVBMC intrabox swap move in its original form processes as follows:

Having a given configuration state, *A*,

1) Randomly select a molecule i to be swapped.

2) Randomly select a second molecule j ($j \neq i$) that acts as a target for the swap move.

3) With a probability of P_{bias}, molecule i is only allowed to swap into the bonded region of molecule j, called the B_{in} state, whereas with a probability of 1-P_{bias}, the molecule i is swapped into the nonbonded region of molecule j, called the B_{out} state.

4) Calculate the potential energy difference, $\Delta E = E_B - E_A$

5) Accept the trial move given the following sets of acceptance probabilities for four types of intrabox swap moves ($A_{in} \rightarrow B_{in}$, $A_{out} \rightarrow B_{out}$, $A_{out} \rightarrow B_{in}$, and $A_{in} \rightarrow B_{out}$):

(a) For $A_{in} \rightarrow B_{in}$ or $A_{out} \rightarrow B_{out}$ cases: These two cases don't involve molecule i entering or leaving the bonded region of the molecule j. Acceptance probability of Metropolis Monte Carlo move is used for these cases.

(b) For the $A_{out} \rightarrow B_{in}$ case: This move results in the formation of a bonded configuration of molecule i and molecule j. In this case, the acceptance rule is given,

$$acc(A_{out} \rightarrow B_{in}) = \min\{1, \frac{(1 - P_{bias})V_{in} \exp(-\Delta E / k_B T)}{P_{bias} V_{out}}\}. \qquad 2\text{-}11$$

(c) For the $A_{in} \rightarrow B_{out}$ case: This move results in the destruction of a bonded configuration of molecule i and molecules j. In this case, the acceptance rule is given,

$$acc(A_{in} \rightarrow B_{out}) = \min\{1, \frac{P_{bias} V_{out} \exp(-\Delta E / k_B T)}{(1 - P_{bias})V_{in}}\}. \qquad 2\text{-}12$$

Given these rules, the AVBMC algorithm improves the bond formation and destruction events in two ways. First, the transition probability for two molecules to meet and form a bonded configuration has been enhanced by allowing direct hopping between bonded and non-bonded regions of molecule i and j. Second, the acceptance probability for the destruction of a bonded configuration of molecule i and j has been enhanced due to the fact that $V_{out} >> V_{in}$.

2.2.4 Umbrella Sampling (US).[4]

Although it is clear that AVBMC enhances cluster formation and destruction in nucleation events by introducing the intrabox swap move, allowing molecules to hop directly between a bonded and a non-bonded region of molecules, by itself this move is not sufficient. A significant sampling problem regarding the critical cluster still remains. In the conventional Metropolis algorithm, the probability of sampling a particular state in configuration space is proportional to its Boltzmann factor. This fact means it takes an extremely long simulation time to sample the critical cluster to obtain good statistical results. For example, the vapor-liquid nucleation barrier height for pure water molecules at 300 K and a vapor density of 2.5×10^{-6} molecules/Å^3, performed by our group is more than 50 k_BT. This value means that the water cluster at its critical size is e^{-50} times less sampled than the monomer, leading to the extremely long simulation time needed for enough sampling over all cluster sizes considered in this nucleation event. The use of umbrella sampling can alleviate these sampling problems at critical cluster size by introducing a biasing potential, which enhances the probability of visiting clusters, and it can be mathematically removed in the later data analysis.

Our choice of a biasing potential is ideally equal to the negative of the nucleation free energy, $-\Delta G(N)$, which allows each cluster size of interest to be sampled roughly evenly in configuration space. This choice of a biasing potential enables maximum possible sampling of each cluster size for a given simulation run ultimately providing good statistics. However, the value of the initial nucleation free energy, $\Delta G(N)$, is not known. It is our final goal to obtain the nucleation free energy (NFE) for each cluster size of interest empirically. This biasing potential, f_{bias}, is determined iteratively using a self-adaptive procedure. For example, initially simulation is performed without a biasing potential (or $f_{bias}=0$). NFE is calculated using the expression in Equation 2-1 for the initial run and then an initial biasing potential can be determined from this

run. Next, another simulation is performed using the calculated initial biasing potential and this process is repeated until all cluster sizes of interest are roughly evenly sampled. This self-adaptive procedure for obtaining a good biasing potential can also be accelerated by obtaining a precise biasing potential for small cluster sizes and extrapolating the data to larger sizes. Finally, the biasing potential is removed in the analysis as follows:

$$\Delta G(N) = -k_B T In \frac{P(N)}{P(1)} - f_{bias}(N) \qquad 2\text{-}13$$

2.2.5 Histogram Reweighting (HR).[5,6]

The efficiency of the AVUS technique is further empowered by incorporating the histogram reweighting (HR) technique which produces information about the thermodynamic state under investigation and for other neighboring thermodynamic states without additional simulations. This technique is based on the independence of the microcanonical density of states for specific simulation conditions such as temperature and chemical potential. In other words, the density of the state for different sets of simulation conditions can be reweighted using the density of the state for given sets of simulation conditions since the microcanonical density of the states of a cluster with a given size N (N-mer) is a function of E (energy) only.

An example of how the nucleation free energy data at different sets of simulation conditions (μ_2,T_2) can be obtained from the information at given sets of simulation conditions (μ_1,T_1) is given below. The microcanonical density of the states for the N-mer is given by the equation:

$$\Omega_N(E) = P_N(E) e^{(-N_1 + E)/k_B T_1} \qquad 2\text{-}14$$

Where $\Omega_N(E)$ is the density of the states with energy E for N-mer, $P_N(E)$ is the probability of observing this N-mer with an energy E, μ_1 is the chemical potential of the monomer, k_B is the Boltzmann constant, and T is the temperature. From this density of the states, new density of the states, $P'_N(E)$, at μ_2 and T_2 can be computed using the following equation:

$$P'_N(E) = \Omega_N(E) e^{[(N_2 - E)/k_B T_2]} \quad \text{2-15}$$

Then total population of *N*-mers at different sets of simulation conditions (μ_2,T_2) can be obtained by integrating over all values of the energy to produce the following equation:

$$P'_N = \int \Omega_N(E) e^{[(N_2 - E)/k_B T_2]} dE \quad \text{2-16}$$

Finally, the nucleation free energy data at (μ_2,T_2) can be calculated as follows:

$$\Delta G'_N = -k_B T_2 In \int \Omega_N(E) e^{[(N_2 - E)/k_B T_2]} dE \quad \text{2-17}$$

Notably, obtaining the new nucleation free energy data at different sets of simulation conditions using histogram reweighting does not require extra computation burdens, because energy is calculated at each Monte Carlo step.

2.3 Application of AVUS-HR Nucleation Algorithm to Two Different Hydrophobic Systems.

We have applied this grand canonical version of a vapor-liquid nucleation algorithm, termed AVUS-HR, to two different hydrophobic relevant systems with small modification. For the first system, which will be described in chapters 3 & 4, we have performed multiple AVUS-HR simulation runs for a methane pair fixed at a certain separation distance inside a hard sphere cavity. By gradually adding water molecules inside this sphere, we could determine the whole association free energy profiles (or NFE) with water molecules as a function of methane pair separation distance. From the association free energy with water molecules at a certain methane pair configuration obtained from AVUS-HR run, their free energy difference between two methane pair configurations can be obtained through the thermodynamic cycles depicted in Figure 2.1.

The benefit of performing multiple simulations rather than one long simulation run can be attributed to alleviating some unique sampling problems. This benefit is especially important when producing whole free energy profiles, because not only does a methane pair require

changes in their separation (or configuration) in the presence of water but, in reverse, the hydration shells requires to be reorganized to accommodate this change. These processes are very time-consuming and sluggish leading to an extremely long simulation time and, ultimately, they may not even be accomplished within the given simulation time.

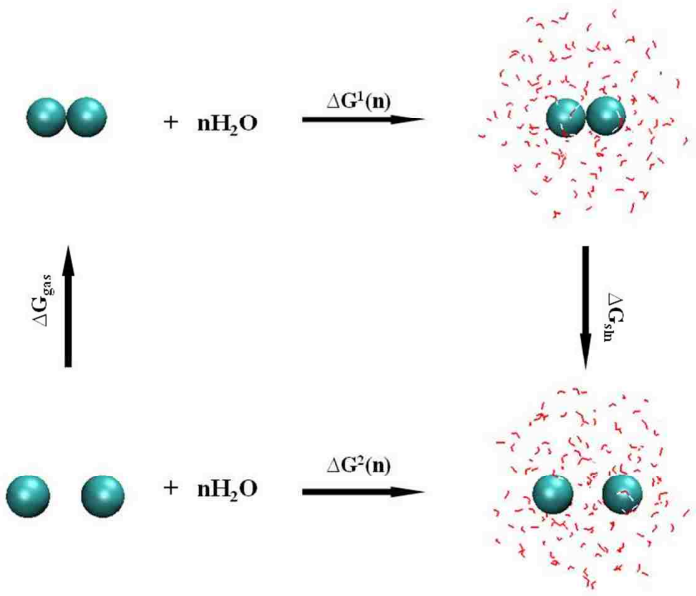

Figure 2.1. Schematic drawing of the thermodynamic cycles used to calculate the free energy difference between the two different solvated methane pair configurations, $\Delta G_{sln}(n)$, inside a cavity. The association free energies with water for these two solute configurations, $\Delta G^1(N)$ and $\Delta G^2(N)$, can be obtained from performing the AVUS-HR simulation runs.

In addition, through a thermodynamic cycle, the free energy difference between two different solute configurations can be calculated from only two AVUS-HR simulation runs even if the two configurations are very different. This spatially indirect pathway connecting the two different solute configurations can be significantly more efficient than other methods such as thermodynamic perturbation or the integration method, in which the free energy difference can be obtained by calculating the free energy change incrementally along the path linking any given two configurations.

For the second system, which will be discussed in chapter 5, we have performed each AVUS-HR simulation run for each separation distance between two infinitely parallel walls by gradual addition of water molecules into the inter-space regions between two walls. Similarly, free energy difference between two different wall configurations can be calculated through the thermodynamic cycles depicted in Figure 2.2.

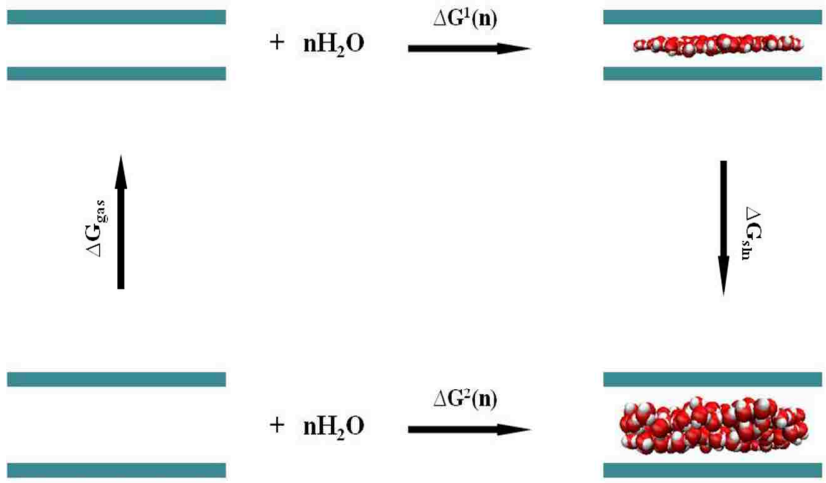

Figure 2.2. Schematic drawing of the thermodynamic cycles used to calculate the free energy difference between the two infinitely parallel walls with different wall separations, $\Delta G_{sln}(n)$, The association free energies with water for these two different wall configurations, $\Delta G^1(N)$ and $\Delta G^2(N)$, can be obtained from performing the AVUS-HR simulation runs.

While most of the researches for large hydrophobic units such as infinitely parallel two walls have focused on the qualitative properties of the system such as layering behaviors of water molecules placed in inter-space regions between two walls, we would like to analyze the quantitative properties for large hydrophobic unit systems providing accurate real values. Ultimately, by utilizing a modified AVUS-HR algorithm we were able to succinctly analyze two different hydrophobic systems more thoroughly than previously reported.

2.4 References.

(1) Chen, B.; Siepmann, J. I.; Klein, M. L., Simulating vapor-liquid nucleation of water: A combined histogram-reweighting and aggregation-volume-bias Monte Carlo investigation for fixed-charge and polarizable models, *J. Phys. Chem. A* **2005**, *109*, 1137-1145.

(2) Chen, B.; Siepmann, J. I.; Chen, B.; Siepmann, J. I., Improving the Efficiency of the Aggregationa-Volume-Bias Monte Carlo Algorithm, *J. Chem. Phys. B* **2001**, *105*, 11275-11282.

(3) Chen, B.; Siepmann, J. I., novel monte carlo algorithm simulating strongly associating fluids:a applications water, hydrogen fluoride, acetic acid, *J. Phys. Chem. B* **2000**, *104*, 8725-8734.

(4) Torrie, G. M.; Valleau, J. P., Monte Carlo free energy estimates using non-Boltzmann sampling: Application to the sub-critical Lennard-Jones fluid, *Chem. Phys. Lett.* **1974**, *28*, 578-581.

(5) Wilding, N. B., critical-point coexistence-curve properties lennard-jones fluid: finite-size scaling study, *Phys. Rev. E* **1995**, *52*, 602-611.

(6) Panagiotopoulos, A., Direct determination of phase coexistence properties of fluids by Monte Carlo simulation in a new ensemble, *Mol. Phys.* **1987**, *61*, 813-826.

(7) Metropolis, N.; Rosenbluth, A. W.; Rosenbluth, M. N.; Teller, A. H.; Teller, E., Equation of State Calculations by Fast Computing Machines, *J. Chem. Phys.* **1953**, *21*, 1087-1092.

(8) Kim, D. Y.; Ramanathan, V., solar radiation budget radiative forcing due aerosols clouds, *J. Geophys. Res.* **2008**, *113*.

(9) Dockery, D. W.; Pope, C. A., 3rd, Acute respiratory effects of particulate air pollution, *Ann, Rev. Public Health* **1994**, *15*, 107-132.

(10) Chkonia, G.; Woelk, J.; Strey, R.; Wedekind, J.; Reguera, D., evaluating nucleation rates direct simulations, *J. Chem. Phys.* **2009**, *130*, 064505.

(11) Frenkel, D. S., B. *Understanding Molecular Simulation*, 2nd ed.; Academic Press: San Diego, 2002.

CHAPTER 3 A NEW APPROACH FOR THE STUDY OF HYDROPHOBIC INTERACTIONS UNDER CONFINEMENT: ENHANCED HYDROPHOBIC ASSOCIATIONS DRIVEN BY ENERGETIC CONTRIBUTION.

3.1 Introduction.

The effects of confinement on hydrophobic interactions are increasingly recognized as important factors for regulating these interactions. In particular, recent research has demonstrated the importance of confinement effects for understanding biological processes in the cellular environment such as the formation of micelles, and biological membranes, and for protein folding/unfolding mechanisms.[1-3] Given that hydrophobic interactions are considered crucial for protein folding/unfolding, the confinement effects on this interaction are likely important for creating and sustaining the overall protein structure. For example, several experimental studies[4-7] have reported that both the stabilities of the folded and unfolded protein states and the folding rate of biological molecules, such as proteins, observed under confined environmental conditions are different from those observed in infinitely dilute solutions, which most previous studies used.

Computer simulation studies[8-11] have also addressed confinement effects on the behavior of nonpolar and/or biological molecules, providing a fundamental understanding at the molecular level of hydrophobic effects. It has been reported that association behaviors of hydrophobic events are enhanced under a confined environment relative to those environments which are not restricted. In particular, two researchers[9, 10] used a methane pair model for small hydrophobic solutes and revealed that confinement enhances the tendency of their association demonstrating that the contact pair is the only stable configuration for their simulation system. Nevertheless, little attention has been given to hydrophobic interaction studies under confinement compared to the number of studies performed in bulk water. In particular, studies of underlying thermodynamic contributions to this association in a confined environment are scarce. The

purpose of this chapter is to reexamine the hydrophobic interactions for a methane pair under confinement through use of our novel method, a combination of AVUS-HR and a thermodynamic cycle. Our data demonstrates the different behaviors of the solvent induced interactions between two methane molecules under a confined environment comparing with the bulk and we further provide the underlying thermodynamic quantities to these different association behaviors under the confined environment. Based on the current scientific literature available, this is the first known computer simulation study dealing with the contributions of entropy and energy to hydrophobic association behaviors for a methane pair under a confined environment. Furthermore, we propose a novel justification for our scientific observation that enhanced hydrophobic association behavior under confined environment appears to be driven by an energetic factor. This observation is in direct contrast to what has been previously observed in bulk water, in which contact pair minimum is driven by entropy in the limitation of small hydrophobic units.[12-14]

3.2 Simulation Methods.

3.2.1 Molecular Models and Monte Carlo Simulations.

Aforementioned in Chapter 2, water-induced hydrophobic interactions for a nonpolar solute pair confined in a nanometer sized hydrophobic cavity were investigated by a combination of AVUS-HR and a thermodynamic cycle as depicted in Figure 2.1. We have slightly modified the grand canonical version of the nucleation algorithm by restricting the formation of water droplets inside the cavity in combination with a fixed pair of nonpolar solute molecules at a certain separation distance. For each solute pair separation, at a distance between 3.5 to 8.0 Å with an interval of 0.1 Å, we performed this modified nucleation simulation by gradually increasing the number of water molecules added inside the cavity. In this confined system, we used a hard sphere cavity with a diameter of 20 Å and gradually added up to 128 water molecules into this

sphere, which gives approximately the same density as the bulk water density under the same conditions (1 atm and 300 K). A methane pair was chosen as a hydrophobic solute model, because it establishes a simple and useful model system that is also widely used in other computer simulation studies of hydrophobic interactions. For this study, methane was modeled by a united atom representation[15] and the TIP4P model[16] was used for water (see Table 3.1). TIP4P is a rigid water molecule represented by four-interaction sites, and it provides more reasonable thermodynamic and structural data for the liquid state of water than a three-site or five-site water model such as SPC, TIP3P, or ST2 according to the water model comparisons generated by Jorgensen et al.[17] All pair interactions were considered during the simulation runs. The Lorenz-Berthelot combing rules were used for the unlike-pair interactions. Equally divided insertion, deletion, translational, and rotational Monte Carlo moves were performed for the water molecules only. An energy-based Stillinger-type cluster criterion was also enforced where a cluster is defined as a group of molecules in which every molecule has at least one neighbor in the group with interaction energy less than $U_{cluster}$. Based on our previous laboratory research, we set this energy cutoff at -260 K for water-water interactions and -30 K for water-methane interactions.

Table 3.1. Lennard-Jones parameters used in our simulations.

	$\mathcal{E}$*[kcal/mol]*	σ*[Å]*
methane-methane	0.294	3.73
oxygen-oxygen	0.155	3.154
methane-oxygen	0.213	3.442

3.2.2 Other Simulation Details.

Bulk NPT Simulations We also performed bulk simulations in the NPT ensemble (given a fixed number of particles N, pressure P, and Temperature T) with a total of 500 water molecules to produce a reference unconfined case for comparison to our confined case simulations. In order to address the system's size effects on the potential of mean force (PMF) for a methane pair in bulk water, we also performed another NPT Monte Carlo simulation using 150 water molecules. Unlike the simulations under confinement, periodic boundary conditions were used for each bulk simulation. For the interaction energy calculation, tail corrections and Ewald summation were used for both bulk simulations. Corresponding (PMFs) have been obtained from Equation 3-1:

$$W(r) = -k_B T Ing(r) \qquad 3\text{-}1$$

Where $g(r)$ is the pair correlation function of two methane solute molecules, k_B is Boltzmann's constant, and T is the absolute temperature in Kelvin. Both bulk simulations were performed at the same basic conditions as the confined case - (1 atm and 300 K).

Contributions of Entropy and Energy to the PMF[12, 13, 18] We further analyzed the contributions of entropy (-TΔS) and energy (ΔU) to the PMF in order to provide a more detailed understanding of the hydrophobic interactions under confinement. S was calculated from the temperature partial derivative of free energy based on the relationship between the equations below:

$$-S(r) = \left(\frac{\partial W(r)}{\partial T} \right)_{V,N} \qquad 3\text{-}2$$

Therefore, $-S(r)$ may be calculated from the free energies at two different temperatures, $T + \Delta T$ and $T - \Delta T$, respectively.

$$-S(r) = \frac{W(r, T+\Delta T) - W(r, T-\Delta T)}{2\Delta T} \qquad 3\text{-}3$$

For our simulations, a ΔT of 0.005 K was applied (a ΔT of 25 K and 10 K were also sampled in order to see the $-S(r)$ dependence on ΔT). The primary disadvantage of this finite difference method (shown in Equation 3-3) is the need to perform the simulations at other two temperatures. However, we obtained PMFs at two other temperatures (T + ΔT and T - ΔT) without the need of additional simulation runs by using histogram reweighting (HR). HR usage allowed us to significantly reduce the simulation time required for the analysis, thereby highlighting one of the advantages of using the AVUS-HR technique in this study. Corresponding contribution of energy (ΔU) to the PMF was finally obtained by following equation:

$$\Delta U(r) = W(r) + T\Delta S(r) \qquad 3\text{-}4$$

Partial Energetic Contributions to the PMF The difference of the water-water interaction term, ΔE_{ww}, and the difference of water-methane interaction term, ΔE_{wm}, were obtained from direct calculations during the simulations. In order to minimize the uncertainty of these interaction energies, we performed calculations on the "flyer". This term is used to indicate that for each Monte Carlo step the obtained water-water and water-methane interaction energies are accumulated separately for each cluster size and later these accumulated sums obtained at each cluster size are averaged by the total number of times visiting that size of clusters. During the simulation run, the total number of times visiting each cluster size for each methane pair configuration is more than 1.4 X 10^9. In addition, this energy calculation on the flyer doesn't require the extra simulation time since water-water and water-methane interaction energies are calculated during every Monte Carlo move.

NVT Monte Carlo Simulation We have also performed another confinement simulation by placing two methane molecules and 128 water molecules inside a hard sphere cavity with a diameter of 20 Å using the NVT ensemble (given a fixed the number of particles N, volume V, and Temperature T) Monte Carlo simulation. Equally distributed translational and rotational

Monte Carlo moves were applied to the water molecules while only translational moves were applied to the methane molecules. The two methane molecules were only allowed to simultaneously move in opposite directions so that the obtained center of mass of these two methane molecules remains at the center of this hard sphere.

Water Orientational Distribution Functions Orientational distribution functions of water dipole directions, with respect to the methane-oxygen vector, for the water molecules was analyzed using following equation:

$$\cos(\theta) = \frac{(r_M - r_O) \quad (r_D - r_O)}{|r_M - r_O||r_D - r_O|} \qquad 3\text{-}5$$

Where r_M is the position vector for the center of mass of the methane molecule, r_O is the position vector of the oxygen molecule, and r_D is a dipole vector of a water molecule (defined as the position vector for the middle of two hydrogen molecules in a water molecule, respectively).

Uncertainty Uncertainties of observed thermodynamic quantities in this study (i.e., the PMF, contributions of entropy and energy to the PMF, and partial energetic terms) were determined as follows:

$$\delta X = \sqrt{\frac{\sum_{i=1}^{N}(X_i - \tilde{X})^2}{N(N-1)}} \qquad 3\text{-}6$$

Where $\tilde{X}$ is an averaged value from all data points obtained, while X_i corresponds to N independent simulation runs. We used 64 independence runs (i.e., each independent run consists of 1×10^7 Monte Carlo steps.) for each methane pair separations considered in this study.

3.3 Results and Discussions.

3.3.1 Potential of Mean Force (PMF).

Figure 3.1 shows the PMF for a methane pair in a rigid hard sphere with 128 water molecules as a function of their separation distance, r, obtained from our method, depicted with the

potential energy for the methane-methane interactions used in this study. We also included the PMF for a methane pair in bulk water obtained from the NPT Monte Carlo simulation with 500 water molecules at 1 atm and 300 K. We set the absolute free energy zero at a separation of 8 Å for all cases.

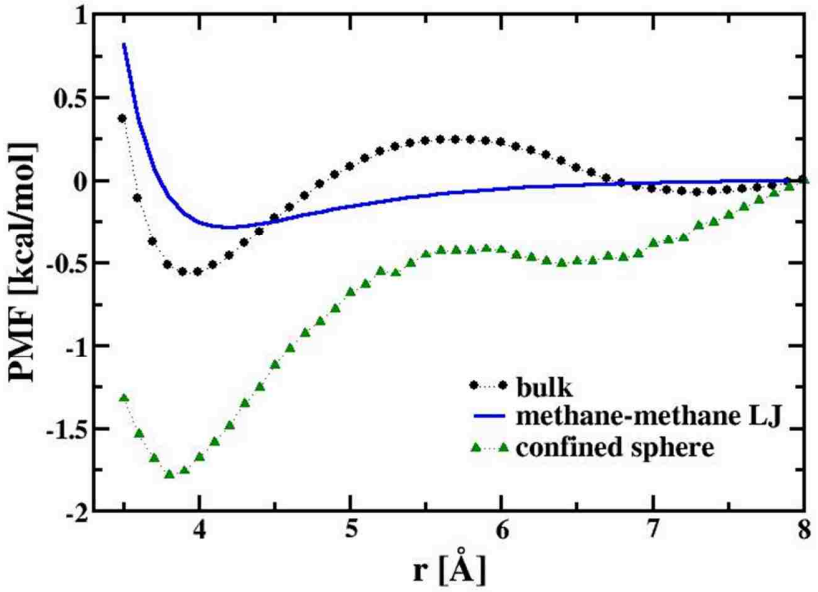

Figure 3.1. The PMF for a methane pair obtained from simulations conducted in a confined nanometer-sized sphere with 128 water molecules (green triangle with dashed line), and in bulk water from NPT Monte Carlo simulation with 500 water molecules (black circle with dashed line). The methane-methane potential energy is also included (blue solid line). Uncertainties are less than $\pm 4.0 \times 10^{-2}$ kcal/mol for the confinement case and less than $\pm 2.0 \times 10^{-2}$ kcal/mol for the bulk at all methane pair separations considered here.

System Size Effect Initially, we tested system size effects on the PMF for a methane pair in bulk water by performing NPT Monte Carlo simulations with 500 and 150 water molecules. The bulk PMFs obtained are displayed in Figure 3.2. The PMFs for both the small and large systems reveal that the well-defined contact pair minimum (CM) is at 3.8 Å. Both have a free energy barrier to contact pair dissociation of approximately 0.92 kcal/mol, and the shallow secondary minimum called the solvent separated minimum (SSM) is at 7.1 Å. Although PMFs obtained from two different sizes of systems are not exactly same, size effect in the PMF is not

significantly big enough to change our conclusions of confinement effect on the PMF. Although Smith and Haymet[12] used different system sizes from those applied here (i.e., 106 and 214 water molecules), they reported that any size effect in the PMF for a methane pair in bulk water is smaller than the noise of the simulations.

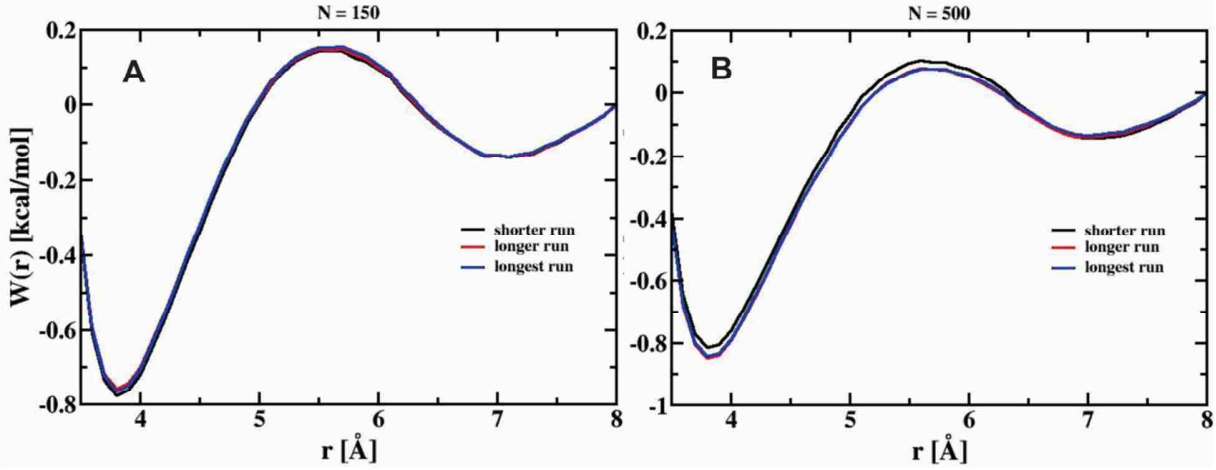

Figure 3.2. Evolution of the PMF as the number of the simulation cycles for a methane pair in bulk water from NPT Monte Carlo simulations with (**A**) 150 and (**B**) 500 water molecules (Monte Carlo steps performed are 1.2×10^7, 1.4×10^7, and 1.6×10^7 for each shorter, longer, and longest run for N=150 case. Monte Carlo steps performed are 4.8×10^7, 6.4×10^7, and 8.0×10^7 for each shorter, longer, and longest run for N=500 case.)

Positions of CM, BH, and SSM The PMFs for both confinement and bulk water simulations show that the global minimum is the contact pair, located at 3.8 Å in Figure 3.1. That minimum appears at a shorter methane pair separation than the minimum position of 4.2 Å in the methane-methane potential energy used here, indicating that the presence of solvent molecules favors shorter separations between two hydrophobic solutes. Although CM in the PMFs for both confinement and bulk water are located at the same methane pair separation, the positions of the secondary minimum (or SSM) are fairly different. The SSM is located at a methane pair separation of 6.4 Å under confinement, much smaller than the methane pair separation of 7.1 Å for the SSM in bulk water. It also shows that the position of the more extended methane pair

configuration is much more affected by confinement than the position of the contact pair configuration. In addition, position of the SSM for confinement is slightly less than twice the methane-oxygen Lennard-Jones distance used in this study, and, consequently, is not literally "solvent separated" whereby one water molecule is directly between two methane molecules.

Relative Free Energies in Confinement vs. Bulk Water As mentioned in the Introduction, the behaviors of hydrophobic interactions under confinement are different from those in bulk water. The relative free energies at positions among CM, barrier height (BH), and SSM for confinement vs. bulk water are noteworthy due to their influence on different behaviors of hydrophobic molecules (and/or biomolecules) in confined (or cellular) environments vs. bulk water (or an infinitely dilute environment). Thus, we have calculated the following terms:

1) the free energy difference between barrier height and contact pair minimum [or dissociation barrier height (DBH)] from $F_{BH} - F_{CM}$
2) the free energy difference between barrier height and solvent separated minimum [or association barrier height (ABH)] from $F_{BH} - F_{SSM}$
3) the relative stability of the CM to the SSM, S_{CM}, from $F_{SSM} - F_{CM}$

All these terms were collected for confinement vs. bulk water and are shown in Table 3.2.

Table 3.2. Free energy differences between two positions among CM, BH, and SSM obtained from simulations for confinement vs. bulk. (Uncertainties are less than $\pm 4.0\times10^{-2}$ kcal/mol for all cases both.)

	$F(r)_{BH}$-$F(r)_{CM}$ [kcal/mol]	$F(r)_{BH} - F(r)_{SSM}$ [kcal/mol]	$F(r)_{SSM}$-$F(r)_{CM}$ [kcal/mol]
bulk	0.85	0.14	0.71
confinement	1.36	0.08	1.28

In Table 3.2, F_{CM}, F_{BH}, and F_{SSM} refer to the association free energy at the CM, BH, and SSM positions, respectively. Although providing an exact quantitative comparison is difficult due to the dependence of hydrophobic interactions on several factors, such as those described in the methodological details and based on the interaction parameters for solvent and solute molecules, generally the DBH and ABH for a methane pair in bulk water are approximately 0.8 to 1.0 kcal/mol and 0.1 to 0.3 kcal/mol, respectively.[19-22] Our values obtained from the bulk water simulation are 0.85 kcal/mol for DBH and 0.14 kcal/mol for ABH. Comparing the bulk values with those for confinement (i.e., 1.36 kcal/mol for DBH and 0.08 kcal/mol for ABH as shown in Table 3.2), the DBH value for confinement is bigger than the bulk value whereas the ABH shows the opposite trend. This comparison of the DBH and ABH values of confinement vs. bulk water reveals that the rate of association is increased while the rate of dissociation is decreased under confined environment comparing to the bulk. More importantly, the contact pair configuration is more stabilized relative to the solvent separated pair under confinement rather than in bulk water. This enhanced preference for hydrophobic association behavior for a methane pair under confinement has been verified by the value of S_{CM} in Table 3.2 (i.e., The S_{CM} values are 0.71 kcal/mol for bulk water and 1.28 kcal/mol for the confinement case.).

Comparisons with Previous Published Studies We have compared our simulation results with two previously published studies[9, 10] for a methane pair under confinement. Both studies ultimately determined that confinement enhances the hydrophobic associations for a methane pair, which is the same conclusion our studies demonstrated. However, an interesting observation resulting from the two earlier studies is the absence of the secondary minimum in the PMFs, whereas our study clearly shows the presence of a shallow SSM. (Figure 3.1) With regard to the study by Vaitheeswaran and Thirumalai,[9] they performed several Monte Carlo simulations for a methane pair confined into four different water droplets ranging in diameter

from 1 to 4 nm. They determined that the independence of the PMFs for a methane pair for a specific sized water droplet is due to the propensity of that methane pair to be at the surface locations of the water droplet. Thus, this importance of surface location on a methane pair of water droplets, in which hydrogen bonding is more disrupted at the surface than in the interior, results in the absence of a second minimum in the PMFs. Therefore, the existence of a secondary minimum in our study can be explained as an artifact from our simulation methods, wherein the two methane molecules are fixed at a certain separation distance, ranging from 3.5 to 8 Å, by restricting the center of the two methane molecules located at the center of a rigid sphere. Regarding the distribution of the methane molecules in a confined sphere, a second study by Rao et al.[10] has reported that two methane molecules are found to lie toward the central region of a reverse micelle with a radius of 14.1 Å. In contrast to our results, however, the SSM was missing in their simulation study. Rao et al. rationalized that a lack of the sufficient water needed to stabilize the solvent separated configuration with one fully hydrated shell was the main reason for not observing a SSM. Based on their calculation, a reverse micelle with a radius of at least 9.1 Å is required to accommodate the solvent separated pair configuration with one full hydration shell. Although the reverse micelle used in their study is big enough to accommodate the solvent separated pair configuration, the water density and hydrogen bonding are significantly reduced at a $r > 6$ Å (r is the distance from the center of reverse micelle) due to the existence of surfactants and sodium counter ions, indicating a lack of sufficient water to stabilize the solvent separated pair configuration. For our simple confinement system, however, the sphere used in our study is big enough to accommodate the solvent separated configuration with one full hydration shell and a dramatic reduction in water density was not shown for all methane pair separations considered. In addition, our single point for a methane pair separation of 6.4 Å, as shown in Figure 3.1, at which our solvent separated minimum appears, supports the fact that

the solvent separated pair configuration of our confined system is solvable at one full hydration shell.

3.3.2 Contributions of Entropy and Energy to the PMF.

Initially, we analyzed the contributions of entropies (-TΔSs) and energies (ΔUs) to the PMF obtained from the finite difference method (FDM) at three different ΔTs of 0.005, 10, and 25 K in order to address the effect of ΔT values on the obtained entropy from FDM. As shown in Figure 3.3 (B), there is no significant difference between the results obtained using different ΔT values. Furthermore, it reveals that the -TΔSs are repulsive at all r, while the ΔUs are attractive resulting in an energetically driven hydrophobic association.

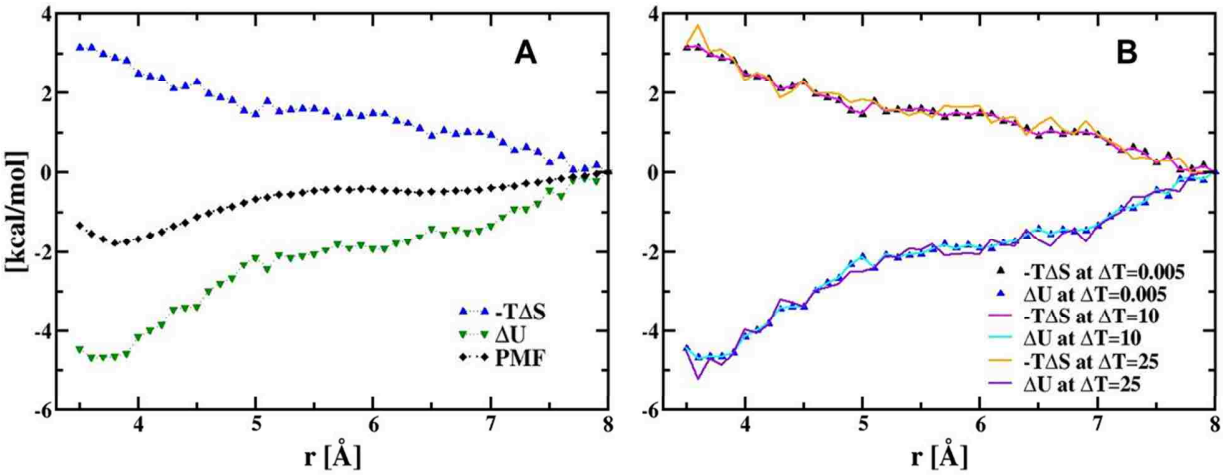

Figure 3.3. (**A**) Contributions of entropy (-TΔS, blue triangle-up with dashed line) to the PMF for a methane with 128 water molecules obtained from a finite difference method (FDA) at ΔT equals to 0.005 K and corresponding energy (ΔU, green triangle-down with dashed line). The PMF is also included (black diamond with dashed line). (**B**) Contributions of entropies (-TΔSs) and energies (ΔUs) at three different ΔTs of 0.005 K, 10 K, and 25K, respectively.

It should be noted that this distinguishable thermodynamic signature is obviously different from observations in bulk water, in which the association behavior of a methane pair is driven by entropy.[12, 13, 18, 23-25] Aforementioned in Chapter 1, current theories support the idea that water structure and hydrogen bonding are not considerably affected by the presence of small hydrophobic solute molecules leading to hydration thermodynamic studies that are dominated by

entropy resulting from restricting spontaneous fluctuations of water molecules near hydrophobic solute molecules. In addition, more favorable entropy at a contact pair over other methane pairs at longer separation distance (i.e., solvent separated pair) appears from the reduction of interfacial surface areas that are accessible to water molecules.

Deviation of our results from the general views on thermodynamic hydrations for small hydrophobic solute molecules can be attributed to the finite size of the confined system. The existence of boundaries indicates that our confined system involves not only hydration thermodynamics resulting from small hydrophobic solutes, but simultaneously those from extended hydrophobic surfaces. This rather complex and specific situation is a likely reason for our unique thermodynamic signatures. In the following chapter sections, we propose that such unique thermodynamic contributions can be explained from the mixture of two different length scale dependent hydration behaviors resulting from the existence of both small and large hydrophobic units.

3.3.3 Water Structure and Hydration Thermodynamics.

Water Oxygen Radial Number Density Profiles We analyzed two types of water oxygen radial number density profiles with regard to the center of either one or two methane molecules. These two types of oxygen radial number density profiles containing the CM, SSM, and 8 Å separations are shown in Figure 3.4. The methane-oxygen radial distribution function for the two individual methane molecules shows that all three methane pair configurations have a clear first hydration shell at 3.6 Å, following a minimum at 4.9 Å. While the shapes of the first hydration shell for the three different separations are similar, those for the second hydration shells (and beyond) are different from each other due to the existence of the sphere boundary. The reduced densities at 7 and 8 Å in the second set of peaks for the SSM and longest methane pair separation of 8 Å are expected given the boundary of the sphere.

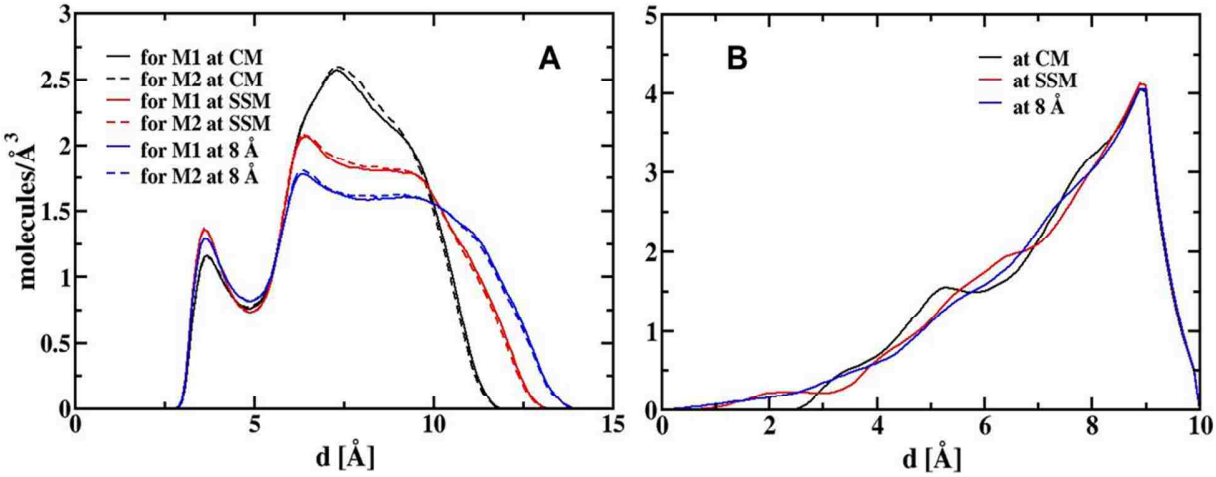

Figure 3.4. Water-oxygen radial number density profiles for either (**A**) the two individual methane molecules or (**B**) the center of two methane molecules in a solute pair (named as M1 and M2) at the CM, SSM, and longest separations. (d [Å] is the radial distance either (**A**) from the center of two methane molecules and (**B**) from methane itself.)

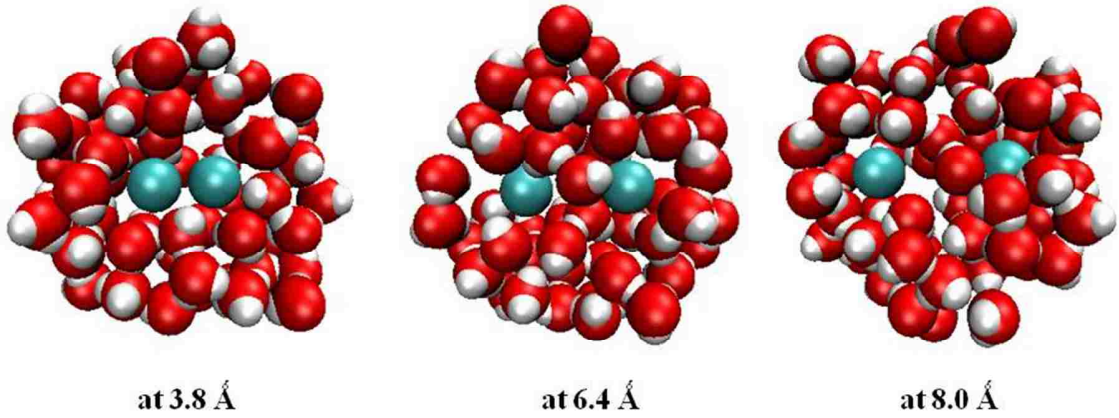

Figure 3.5. Snap shots for three different methane pair configurations at their CM, SSM, and 8.0 Å. Only 54 water molecules are displayed for each configuration.

As shown in Figure 3.4, the CM has a more complete second hydration shell than the other two separations, indicating that existence of boundary of a hard sphere makes it more difficult to complete the formation of a hydration shell beyond the first shell as r increases from the CM, to SSM, and to 8 Å. Figure 3.5 depicts snap shots taken from three different methane pair configurations at the CM, SSM, and 8 Å, with only 54 water molecules displayed in order to show clear solvation structures near them. These snap shots also verify that the second hydration

shell at the CM is more complete than those at the two longer separations. Although the quantities of the number of water molecules near the boundary are similar in all three different methane pair configurations as shown in Figure 3.4 (B), the effects of the boundary on the extent of forming a second solvation shell is different for each methane pair configuration.

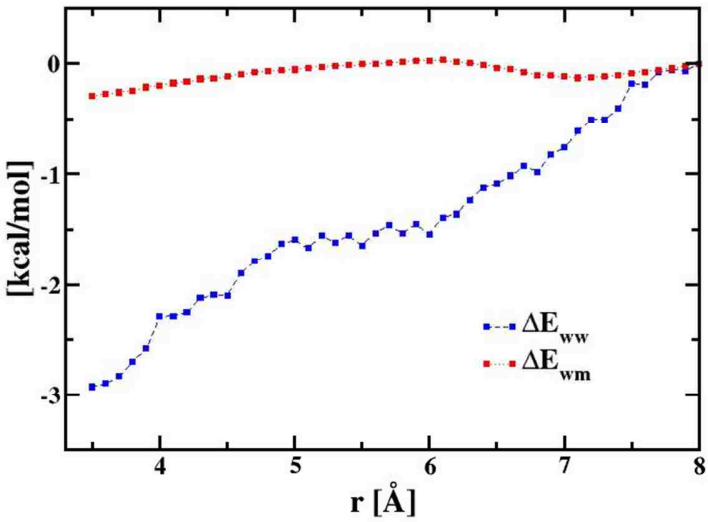

Figure 3.6. The partial energetic terms of the PMF for a methane pair with 128 water molecules at 300 K. The difference of the water-water interaction energy term, ΔE_{ww} (blue square with dashed line), and the difference of water-methane interaction energy term, ΔE_{wm} (red square with dashed line) are calculated directly during simulation performance. Uncertainty for the difference of water-methane interaction energy is less than $\pm 1.5\times10^{-2}$ kcal/mol and the difference of water-water interaction energy is less than ±0.45 kcal/mol.

Analysis of Solvent-Solvent and Solvent-Solute Interaction Energies We further analyzed the difference of the water-water interaction energy, $\Delta E_{ww,}$ and the difference of the water-methane interaction energy, $\Delta E_{wm.}$ Figure 3.6 shows that ΔE_{ww} becomes less attractive as r increases while ΔE_{wm} nears zero at all pair separations, indicating ΔE_{ww} is the major contributor to the energy. The observed behavior for these energetic terms is different from those in bulk water. According to a computer simulation study performed by Tsunekawa et al.,[26] the difference of the water-water interaction energy is almost zero for all r considered in their study, supporting an idea of water structure and hydrogen boding are not significantly affected by methane pair

configurations in the bulk. The observed behavior of ΔE_{ww}, in which energy becomes more negative as r decreases, can be explained from boundary effects on the formation of the second hydration shell as a function of r; a more complete second hydration shell forms as r becomes shorter resulting in a more favorable ΔE_{ww} at a shorter r.

Water Orientational Distribution Functions Figure 3.7 shows the orientational distribution functions of the water dipole directions with respect to the methane-oxygen vector only for the water molecules in both the first and the second hydration shells for the CM, SSM, and 8.0 Å obtained from Equation 3-5. For all three configurations, the first hydration shell is defined with a $|r_M - r_O| \leq 4.9$ Å. For our convenience, we divided the second shell into two regions defined by either 5.0 Å $< |r_M - r_O| \leq 8.0$ Å (called SS1) or 8.0 Å $< |r_M - r_O|$ (called SS2).

The orientational distribution functions for a water dipole in the first shell show peaks at similar positions (i.e, $\cos(\theta)$=-0.36 Å for CM, $\cos(\theta)$=-0.38 Å for SSM, and $\cos(\theta)$=-0.34 Å for 8 Å), indicating a water dipole for all three methane pair configurations pointing away from the hydrophobic solute because it cannot make a hydrogen bonding with water molecules. Figure 3.7(**B**) shows broad peaks for the second shell with a 5.0 Å $< |r_M - r_O| \leq 8.0$ Å around $\cos(\theta)$= 0.25 Å for all three separations. These orientaional distribution functions for water molecules beyond the first hydration shell reveal that confinement induces a more ordered water structure when compared to bulk water. For bulk water, the line for a water dipole beyond the first hydration shell appears flat while the line shapes of the first and second hydration shells are identically curved under a confined environment. This more ordered (or oriented) structure of water molecules under confinement can be attributed to the existence of a boundary surface resembling a vapor-liquid like interface, which makes water molecules near the boundary point away from the hydrophobic boundary of the sphere. The boundary effects on water orientation can be seen more clearly for 8.0 Å $< |r_M - r_O|$ in Figure 3.7(**B**). Furthermore, this figure shows the

CM separation has a higher peak than the SSM or 8Å, indirectly supporting a more ordered water structure at the CM separation over the SSM or 8Å, and ultimately resulting in a relatively unfavorable entropy at the CM.

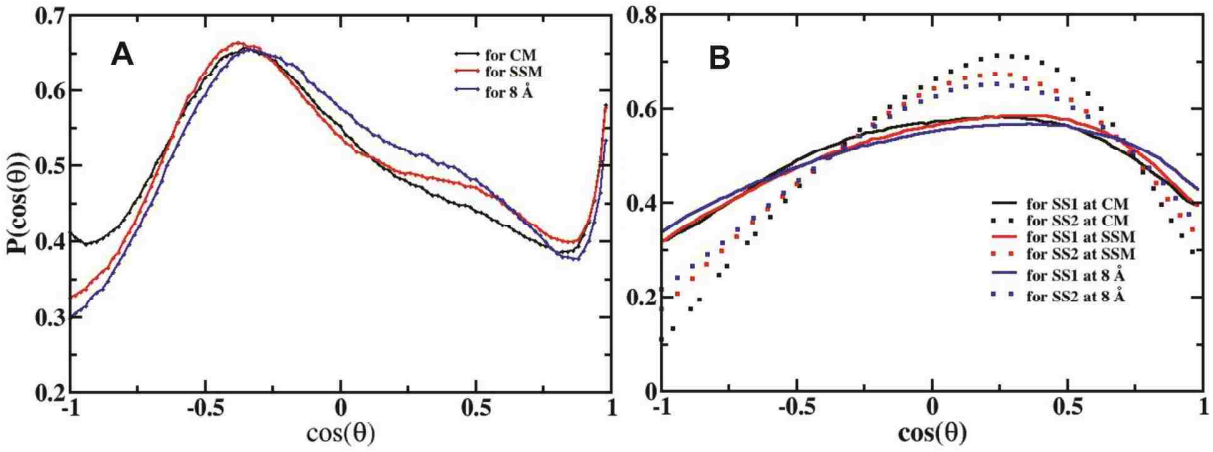

Figure 3.7. Orientational distribution functions for the water dipole directions with respect to the methane-oxygen vector for the water molecules (**A**) in the first solvation shell and (**B**) in the second solvation shell (SS1 and SS2) at the CM, SSM, and the longest separation of 8 Å.

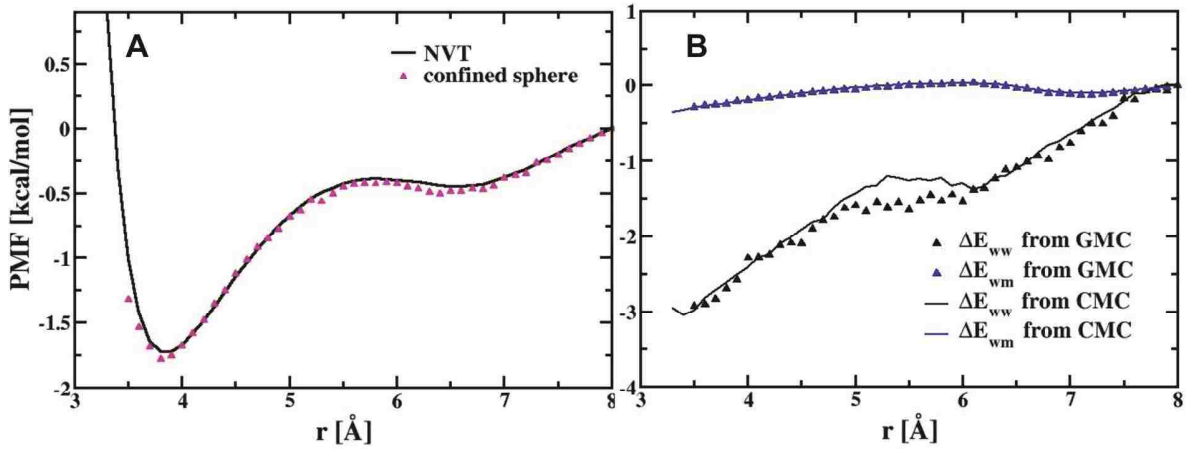

Figure 3.8. (**A**) The PMFs for a methane pair confined in a hard sphere with a diameter of 20 Å obtained from NVT and a modified grand canonical version of the Monte Carlo simulations and (**B**) their partial energetic contributions.

3.3.4 Reliability of Our Simulation Methods for Hydrophobic Interaction Study.

In order to demonstrate the reliability of our obtained results, we also performed another simulation run at constant volume and temperature with 128 water molecules. Figure 3.8 shows that these two PMFs are in fairly good agreement with each other, both showing an enhanced

tendency for hydrophobic solute association under confinement. Moreover, the two systems show the same trends of ΔE_{ww} and ΔE_{wm} over all r.

3.4 Conclusions.

We have applied our new simulation method, a combination of the AVUS-HR nucleation algorithm and a thermodynamic cycle, to the investigation of water-mediated interactions between two hydrophobic solute molecules, a pair of methane molecules, placed in a hard sphere with a diameter of 20 Å. We determined that the association behavior of a pair of methane molecules is enhanced under a confined environment when compared with that in the bulk. This enhanced hydrophobic association has also been reported in earlier simulation studies with hydrophobic and/or hydrophilic cavities of a similar size to our confined environment of a hard sphere. By restricting the distribution of the two methane molecules in the central region of a sphere, we predicted an effect similar to the reserve micelle in hydrophobic interactions, which produces a more realistic cell-like environment.

Given the inherent difficulties for obtaining entropy contributions to hydrophobic interactions in computer simulations, there are not many published studies of these quantities to compare with interaction itself. To the best of our knowledge, there have been no computer simulation studies dealing with the contributions of entropy and energy to the hydrophobic interactions for a methane pair in a confined environment although several simulation studies exist for bulk water. By taking advantage of our method, the contributions of entropy and energy were analyzed in our study without additional simulation runs through a histogram reweighting method. We found that energy is getting more favorable as inter-solute distance, r, decreases, leading to energetically-driven hydrophobic associations. This finding is different from computer simulation studies performed in bulk water where contact pair minimum is driven by entropy due to reduced surface area accessibility to water molecules between the two methane molecules. We

conclude that due to the dependence of microsolvation behaviors on the location of a methane pair inside a hard sphere, the extent of boundary effects on the formation of hydration shells near methane molecules are different. Furthermore, existence of the boundary of the hard sphere makes it harder to complete hydration shells beyond the first one as inter-solute distance, r, increases creating an energy driven hydrophobic association from a more favorable water-water interaction energy. In addition, unfavorable entropy at the CM can be explained from a more ordered second hydration shell at the CM rather than a longer separation.

3.5 References.

(1) Chandler, D., Theory of hydrophobic effect, *J. Chem. Phys.* **1977**, *67*, 3683-3704.

(2) Dill, K. A., Dominant forces in protein folding, *Biochemistry* **1990**, *29*, 7133-7155.

(3) Kauzmann, W., Some factors in the interpretation of protein denaturation, *Adv. Protein Chem.* **1959**, *14*, 1-63.

(4) Eggers, D. K.; Valentine, J. S., Molecular confinement influences protein structure and enhances thermal protein stability, *Protein Sci.* **2001**, *10*, 250-261.

(5) Ravindra, R.; Zhao, S.; Gies, H.; Winter, R., Protein encapsulation in mesoporous silicate: the effects of confinement on protein stability, hydration, and volumetric properties, *J. Am. Chem. Soc.* **2004**, *126*, 12224-12225.

(6) Campanini, B.; Bologna, S.; Cannone, F.; Chirico, G.; Mozzarelli, A.; Bettati, S., Unfolding of Green Fluorescent Protein mut2 in wet nanoporous silica gels, *Protein Sci.* **2005**, *14*, 1125-1133.

(7) Bolis, D.; Politou, A. S.; Kelly, G.; Pastore, A.; Temussi, P. A., Protein stability in nanocages: a novel approach for influencing protein stability by molecular confinement, *J. Mol. Biol.* **2004**, *336*, 203-212.

(8) Vaitheeswaran, S.; Reddy, G.; Thirumalai, D., Water-mediated interactions between hydrophobic and ionic species in cylindrical nanopores, *J. Chem. Phys.* **2009**, *130*, 094502.

(9) Vaitheeswaran, S.; Thirumalai, D., Hydrophobic and ionic interactions in nanosized water droplets, *J. Am. Chem. Soc.* **2006**, *128*, 13490-13496.

(10) Rao, P. V.; Gandhi, K. S.; Ayappa, K. G., Enhancing the hydrophobic effect in confined water nanodrops, *Langmuir* **2007**, *23*, 12795-12798.

(11) Homouz, D.; Hoffman, B.; Cheung, M. S., Hydrophobic interactions of hexane in nanosized water droplets, *J. Chem. Phys. B* **2009**, *113*, 12337-12342.

(12) Smith, D. E.; Haymet, A. D. J.; David E. Smith, A. D. J. H., Free energy, entropy, and internal energy of hydrophobic interactions: Computer simulations, *J. Chem. Phys.* **1993**, *98*, 6445-6454.

(13) Smith, D. E.; Zhang, L.; Haymet, A. D. J., Entropy of association of methane in water: a new molecular dynamics computer simulation, *J. Am. Chem. Soc.* **1992**, *114*, 5875-5876.

(14) Haymet, A. D. J., free energy, entropy, internal energy hydrophobic interactions: computer simulations, *J. Chem. Phys.* **1993**, *98*, 6445-6454.

(15) Jorgensen, W. L.; Madura, J. D.; Swenson, C. J., Optimized intermolecular potential functions for liquid hydrocarbons, *J. Am. Chem. Soc.* **1984**, *106*, 6638-6646.

(16) Jorgensen, W. L., Quantum and statistical mechanical studies of liquids. 10. Transferable intermolecular potential functions for water, alcohols, and ethers. Application to liquid water, *J. Am. Chem. Soc.* **1981**, *103*, 335-340.

(17) Jorgensen, W. L.; Chandrasekhar, J.; Madura, J. D.; Impey, R. W.; Klein, M. L., comparison simple potential functions simulating liquid water, *J. Chem. Phys.* **1983**, *79*, 926-935.

(18) Ghosh, T.; Garcia, A. E.; Garde, S., enthalpy entropy contributions pressure dependence hydrophobic interactions, *J. chem. Phys.* **2002**, *116*, 2480-2486.

(19) Van Belle, D.; Wodak, S. J., Molecular dynamics study of methane hydration and methane association in a polarizable water phase, *J. Am. Chem. Soc.* **1993**, *115*, 647-652.

(20) Sobolewski, E.; Makowski, M.; Czaplewski, C.; Liwo, A.; Ołdziej, S.; Scheraga, H. A., Potential of mean force of hydrophobic association: dependence on solute size, *J. Phys. Chem. B* **2007**, *111*, 10765-10774.

(21) Rank, J. A.; Baker, D., Contributions of solvent-solvent hydrogen bonding and van der Waals interactions to the attraction between methane molecules in water, *Biophys. Chem.* **1998**, *71*, 199-204.

(22) Dang, L. X., Potential of mean force for the methane-methane pair in water, *J. Chem. Phys.* **1994**, *100*, 9032-9034.

(23) Némethy, G.; Peer, W. J.; Scheraga, H. A., Effect of protein-solvent interactions on protein conformation, *Annual review of biophysics and bioengineering* **1981**, *10*, 459-497.

(24) Hummer, G.; Paulaitis, M. E., hydrophobic interactions: conformational equilibria association non-polar molecules water, *Faraday Discuss.* **1996**, *103*, 125-139.

(25) Shimizu, S.; Chan, H. S., Configuration-dependent heat capacity of pairwise hydrophobic interactions, *J. Am. Chem. Soc.* **2001**, *123*, 2083-2084.

(26) Tsunekawa, N.; Miyagawa, H.; Kitamura, K.; Hiwatari, Y., A study water-water interactions hydrophobic association molecular dynamics simulation optimized umbrella sampling method, *J. Chem. Phys.* **2002**, *116*, 6725-6730.

CHAPTER 4 EVOLUTION OF THERMODYNAMICS FOR A METHANE PAIR DURING ADDING EVENTS OF SOLVENT MOLECULES INTO A RIGID HARD SPHERE.

4.1 Introduction.

Another benefit, not discussed in the previous chapter, of using the modified grand canonical version of the vapor-liquid nucleation algorithm, is to interrogate the role of solvent molecules by monitoring the evolution of microsolvation thermodynamics for a methane pair with regard to solvent number and their separation distance during gradual adding events of water molecules into a rigid hard sphere. The study of microsolvation thermodynamics in our project involves analyzing the association free energy (or PMF), contributions of entropy and energy to the PMF, and partial energetic terms. In particular, previously we succeeded in demonstrating the evolution of water mediated interactions for various ion pairs as a function of their separation distance during adding events of solvent molecules through our novel thermodynamic method.[1] For example, we obtained a water mediated interaction of an ion pair of Na^+ and Cl^-, which was similar to that in a bulk-phase system performed by Masunov and Lazaridis,[2] when adding only 60 water molecules. We further demonstrated that attractive interactions between two like charged ions could be induced by adding an appropriate number of water molecules.

We reported results focusing on different association behaviors for a methane pair under confinement from those in bulk water in previous chapter. As a continuing research on the excluded volume effects by a fixed boundary on association behaviors of a methane pair under confinement, in this chapter we will show the following observations of evolution of microsolavtion behaviors for a small hydrophobic solute pair in a rigid hard sphere: 1) how solvent (water) mediated interactions of a methane pair evolve and 2) what would be the key and underlying thermodynamic contributions for the evolution of these interactions during gradual adding events of solvent molecules inside a hard cavity.

4.2 Simulation Methods.

The simulation methods used in this chapter were discussed in detail in the previous chapter. Briefly, we gradually added 1 to 128 water molecules inside a rigid hard sphere containing a methane pair fixed at a given separation ranging from 3.5 to 8 Å. The calculations for the water mediated interactions (or PMFs) were performed by using a combination of the AVUS-HR technique (for evaluation of association free energy with water molecules at a specific methane pair separation) and a thermodynamic cycle (for obtaining the difference in the association free energy between two different methane pair configurations). We also performed analysis for other thermodynamic properties and for the structure of water molecules as the solvent number increases to acquire a molecular level understating of the hydration filling thermodynamics of a rigid hard sphere according to different methane pair configurations.

Evolution of Entropy and Energy Contributions to the PMF Based on the finite difference method,[3, 4] we analyzed the contributions of entropy ($-T\Delta S$) and the corresponding energy (ΔU) to the PMF with respect to both the methane pair separation and the solvent number added into a hard sphere.

Water-oxygen Radial Number Density Profiles The structure of the water molecules added into a hard sphere were investigated by analyzing oxygen radial number density profiles with respect to the center of the two methane molecules as well as to the methane molecule itself. Density profiles were generated during simulation runs by averaging all possible molecular configurations formed with regard to the number of water molecules added into a hard sphere.

Partial Energetic Terms The difference of the water-water interaction energy term, ΔE_{ww}, was obtained by summation of the difference of the water-water Lennard-Jones interaction and the difference for the water-water electrostatic interaction terms. The difference of the water-

methane interaction energy term, ΔE_{wm}, was also calculated. All partial energetic terms were analyzed by direct calculations during running the simulation.

4.3 Results and Discussions.

For reader clarity and efficient comparison, the evolution of water mediated interactions of a methane pair and their underlying thermodynamic contributions to these evolving interactions with regard to separation distance, r, for a different solvent number, n, are displayed in two sections.

4.3.1 Evolution of Hydration Thermodynamics and Water Structures Inside a Hard Sphere Filled with 10 to 60 Water Molecules.

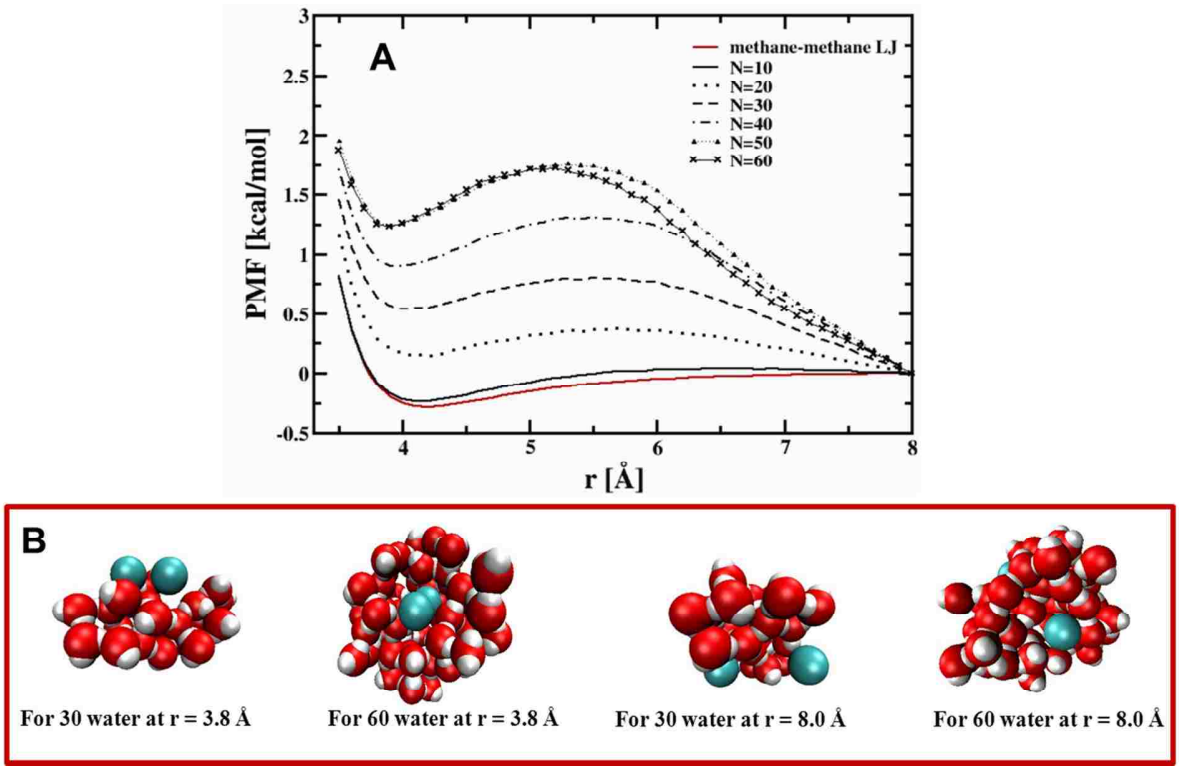

Figure 4.1. (**A**) Evolutions of the PMF for a methane pair as a function of their separation distance, r, from 10 to 60 water molecules. N is the number of water molecules added into a hard sphere. (**B**) Four snap shots taken from movie files for 30 and 60 water molecules at r of 3.8 Å and 8 Å, respectively.

Figure 4.1 shows the evolution of the PMF from 10 to 60 water molecules and includes four snap shots taken from movie files for a certain cluster size (or certain number of solvent

molecules) at r of 3.8 Å and 8 Å. The absolute zero value was set at the longest separation of 8 Å for all cases considered in this study.

Initially, addition of 10 water molecule does not change the PMF significantly when compared to a bare methane pair. Subsequent addition of water molecules, as shown in Figure 4.1, causes the PMFs at short separations (i.e., less than r = 5.5 Å) to incrementally increase up to 60 molecules, where the contact pair minimum (CM) has a maximum positive value among all the considered number of water molecules. This observation indicates that the methane pair configuration at a short r becomes less stable relative to the reference configuration of 8 Å. On the other hand, the shoulder starts to appear at 30 water molecules, and continue to becoming more unfavorable until 50 or 60 water molecules.

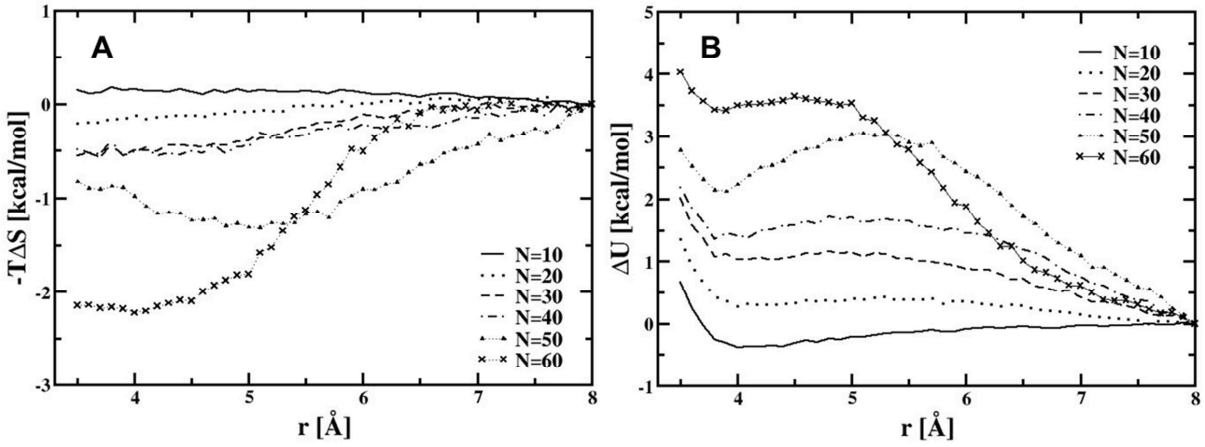

Figure 4.2. (**A**) Evolutions of the contributions of the entropy (-TΔS) to the PMF obtained from the finite difference method and (**B**) the corresponding energy (ΔU) to the PMF with addition of 10 to 60 water molecules.

The evolution behaviors of water mediated hydrophobic interactions between two methane molecules can be shown as the result of interplay between two corresponding thermodynamic contributions of entropy and energy. When 10 to 60 water molecules are added, as shown in Figure 4.2, entropies become more favorable while energies become less favorable at a short r

with increasing solvent number. This observation demonstrates that an unfavorable energy is the more important contributing factor for determining the total shape of the PMF.

In order to show the dependence of microsolvation behaviors (i.e., contributions of entropy and energy to the PMF) on methane pair configuration inside a hard sphere, we analyzed water structures by averaging out their positions with respect to the center of two methane molecules, as well as the methane itself at two methane pair separations. We used one separation set at 3.8 Å to represent the short r, and another set at 8 Å to represent the long r. For 8 Å case as shown in Figure 4.3, a water molecule can access the space between two methane molecules and continue to fill that space until 50 water molecules added. On the contrary, for 3.8 Å case a water molecule cannot enter the space between two methane molecules.

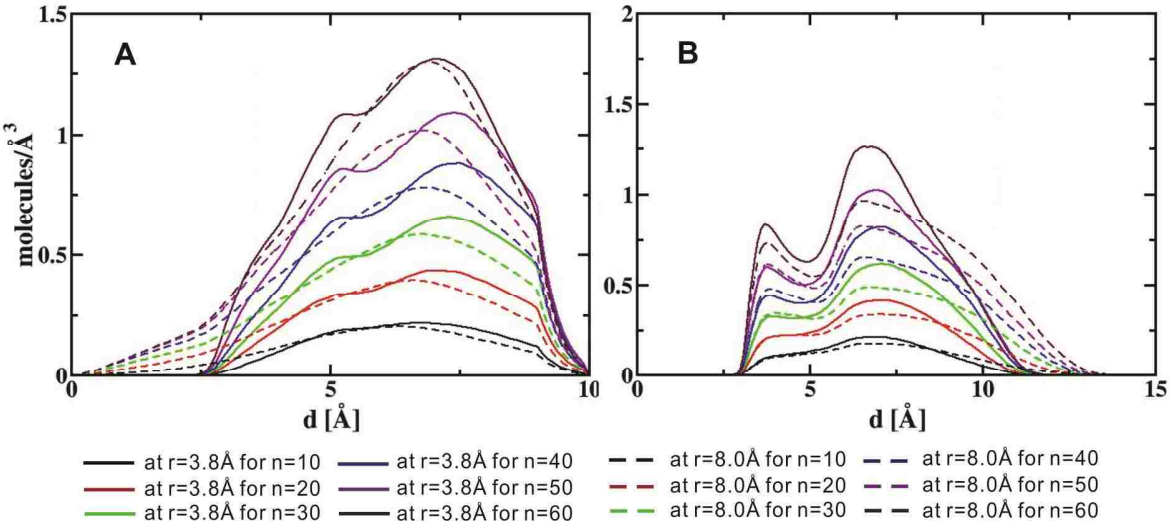

Figure 4.3. Water oxygen radial number density profiles with respect to either (**A**) the center of two methane molecules or (**B**) the methane itself from 10 to 60 water molecules added into a hard sphere for a methane pair configuration at r of 3.8 Å and 8Å. (d [Å] is the radial distance either from (**A**) the center of two methane molecules and (**B**) the methane itself.)

The water molecule accessibility to the space between two methane molecules is considered as a major factor in determining the different microsolvation behaviors between a short r and long r as shown in snap shots depicted in Figure 4.1. For example, for the case of a short r, it

seems like that a pair of methane molecules on contact functions as one big hydrophobic solute molecule, making water molecules added simultaneously fill the half of the sphere first and solvate one big hydrophobic solute molecule composed of actually two methane molecules. Additionally, for this short r case, water molecules can be located relatively near the boundary of a hard sphere (see Figure 4.3 (**A**)) producing more broken hydrogen bonds between water molecules due to the near existence of big hydrophobic unit of the boundary ultimately leading to relatively both unfavorable water-water interactions and favorable entropy contribution. These behaviors of relatively unfavorable water-water interaction energy and relatively favorable entropy contribution reach a maximum around 60 water molecules. On the other hand, due to the accessibility of the space between two methane molecules for a long r, water added into a hard sphere can fill the inside region of the hard sphere making a stronger water-water network. This results in relatively much favorable water-water interaction energy and a less favorable entropy contribution than for a short r.

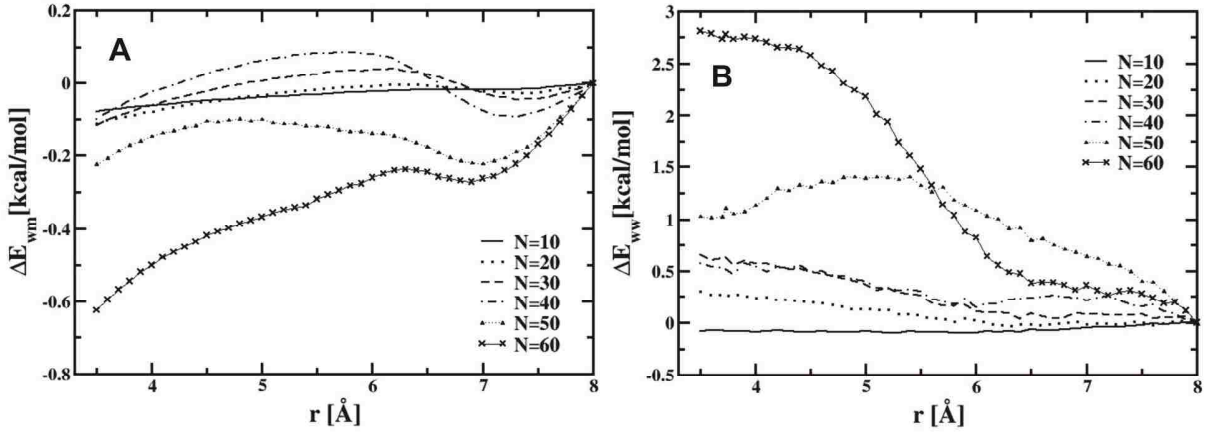

Figure 4.4. (**A**) Evolution of the difference of water-methane interaction energy, ΔE_{wm}, and (**B**) the difference of water-water interaction energy, ΔE_{ww}, as a function of methane pair separation distance, r, for 10 to 60 water molecules.

This relatively more cooperative water network formation observed for a long r rather than a short r can also be proven by analyzing the evolution of the difference in partial energetic

contributions to the PMF. Figure 4.4 shows the difference for both the water-water interaction energy term, ΔE_{ww}, and for the water-methane interaction energy term, ΔE_{wm} for 10 to 60 water molecules. Globally, the graphs demonstrate that when the water molecules are added up to 60, the ΔE_{ww} becomes more unfavorable for a methane pair with a short r rather than for long r. This analysis establishes that the evolutionary behavior of the ΔE_{ww} is a major contributor to the evolutionary behavior of the energy contribution to the PMF for 10 to 60 water molecules.

4.3.2 Evolution of Hydration Thermodynamics and Water Structures Inside a Hard Sphere Filled with 70 to 128 Water Molecules.

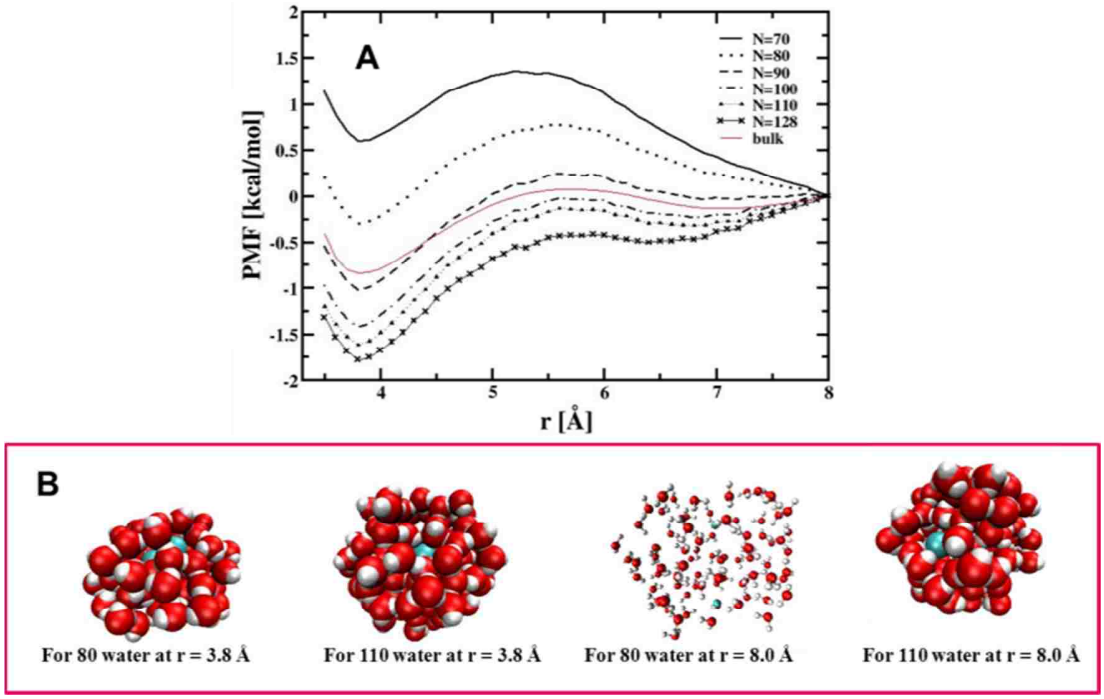

Figure 4.5. (**A**) Evolution of the PMF for a methane pair from 70 to 128 water molecules added into a hard sphere, and (**B**) four snap shots taken from movie files for 80 and 110 water molecules at r of 3.8 Å and 8 Å.

The PMF, which becomes more unfavorable by adding up to 60 water molecules at a short r, continues to behave less favorably upon adding 10 more water molecules inside a hard sphere. Finally, when 80 water molecules are added into a sphere, the contact pair minimum (CM) becomes relatively more stable than the reference state, set at 8 Å, and has a slightly negative

value (i.e., -0.26 ± 0.02 kcal/mol). This CM continues to be more stable when adding up to 128 water molecules and has a free energy of -1.77 ± 0.04 kcal/mol, as shown in Figure 4.5.

We also displayed some snap shots taken from movie files for the addition of 80 and 110 water molecules at r of 3.8 Å and 8 Å, respectively. For the 80 water molecule case at 3.8 Å, the snap shots show that the first solvation shells for two methane molecules in contact are almost completely formed. Thus, when more than 80 water molecules are added into a hard sphere, they are fulfilling another half of the sphere and simultaneously forming a second solvation shell for the one big hydrophobic solute surface when considering that two methane molecules act as one big hydrophobic solute molecule.

In contrast, for the 80 water molecule case at r of 8.0 Å, a dumbbell-like water cluster having two holes at the surface of the two methane molecules is formed. This observation is a result of gradual filling of the water molecules inside the space between the two methane molecules at a separation of 8.0 Å. These further added water molecules continue to fulfill the holes and complete the formation of the first solvation shell for uncovered surfaces of the two methane molecules.

The two different types of oxygen radial distribution functions depicted in Figure 4.6 support the different microsolvation behaviors taken from the four snap shots at two different methane pair configurations (Figure 4.5 (**B**)). For example, peaks at round 3.6 Å corresponding to the first solvation shell in methane-oxygen radial distribution profiles with regard to the methane molecule itself for a short r appear not to change much after 80 water molecules are added. Additionally, another profile with regard to the center of the two methane molecules separated at 3.8 Å in Figure 4.6 (**B**) shows that peaks around 5 Å, corresponding to the first solvation shell, don't change much after 80 water molecules are added. Both analyses indicate that formation of the first solvation shell for a methane pair separated at 3.8 Å has been completed after the

addition of 80 water molecules. For a long r, on the other hand, the constant increase of peaks at 3.6 Å in the methane-oxygen radial distribution profiles supports the fact that there is gradual formation of the first hydration shell for two methane molecules separated at r of 8.0 Å until all 128 water molecules are added.

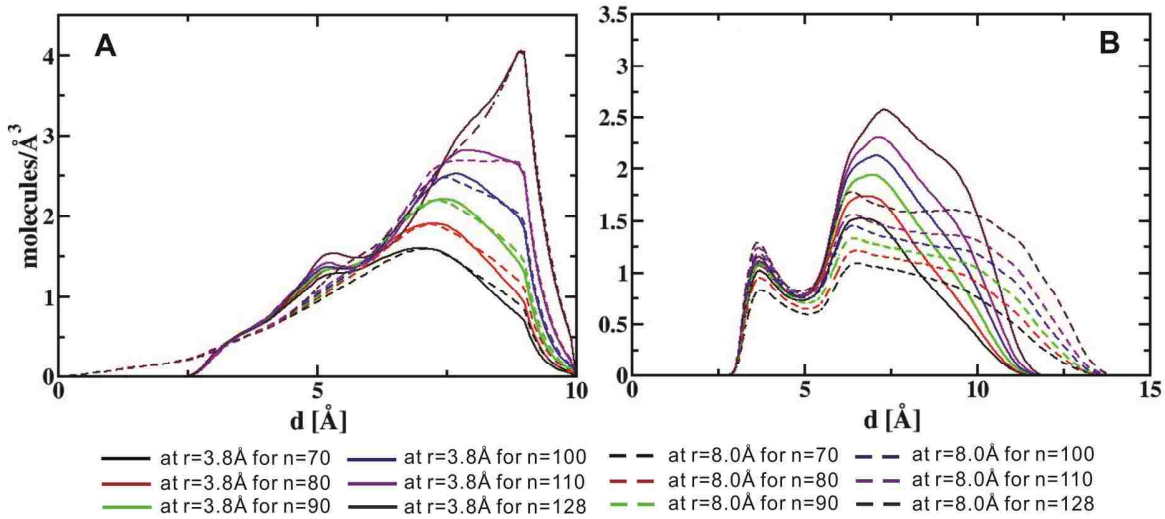

Figure 4.6. Water oxygen radial number density profiles with respect to either (**A**) the center of two methane molecules or (**B**) the methane itself when 70 to 128 water molecules are added into a hard sphere cavity for a methane pair configuration at 3.8 Å and 8Å. (d [Å] is the radial distance either (**A**) from the center of two methane molecules and (**B**) from methane itself.)

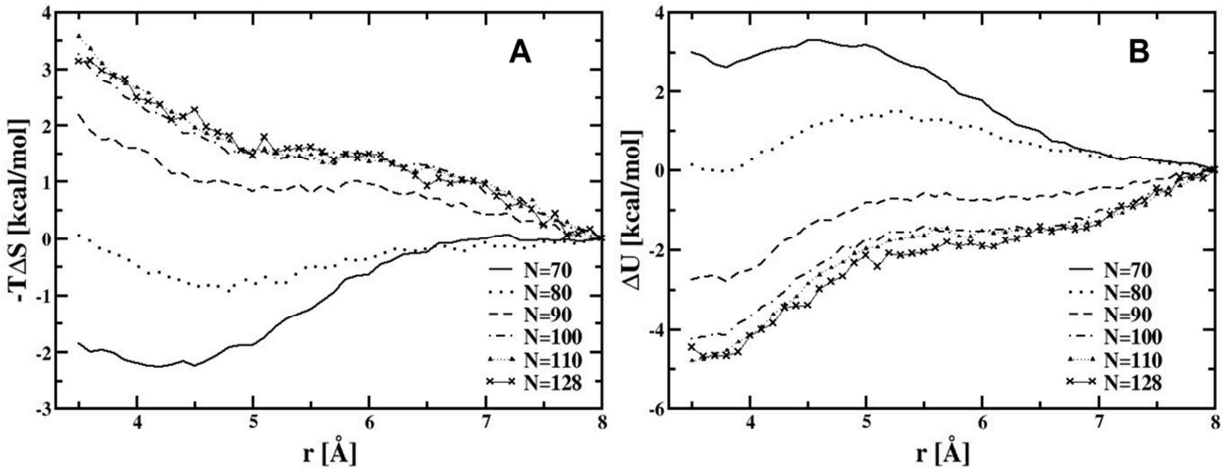

Figure 4.7. Evolution of the contributions of (**A**) the entropy (-TΔS) and (**B**) the energy (ΔU) to the PMF with the addition of 70 to 128 water molecules.

Figure 4.7 shows the contributions of the entropy (-TΔS) and the energy (ΔU) to the PMF from 70 to 128 water molecules. At 70 water molecules, compared to 60 water molecules, the

entropy contribution is very similar over all r values. The energy contribution, however, is slightly less positive at a short r for 70 water molecules than for 60 water molecules, which results from the increased negative values for the water-methane interaction energy at a short r for 70 versus 60 water molecules. When adding 10 more water molecules, the entropy starts to become less favorable, while the energy continues to be more favorable at a short r. Ultimately, adding more water molecules produces an almost flat like entropy and energy contribution to the PMF over all r values.

When adding more than 90 water molecules, the entropies are becoming more positive, while the energy contributions are becoming more negative at a short r. Therefore, after the addition of 80 water molecules, a more favorable PMF at the CM than at 8.0 Å can be attributed to the more favorable energy contributions at the CM than at 8.0 Å. Further, this more favorable energy can be explained as a result of the more favorable ΔE_{ww} at the CM than at 8.0 Å.

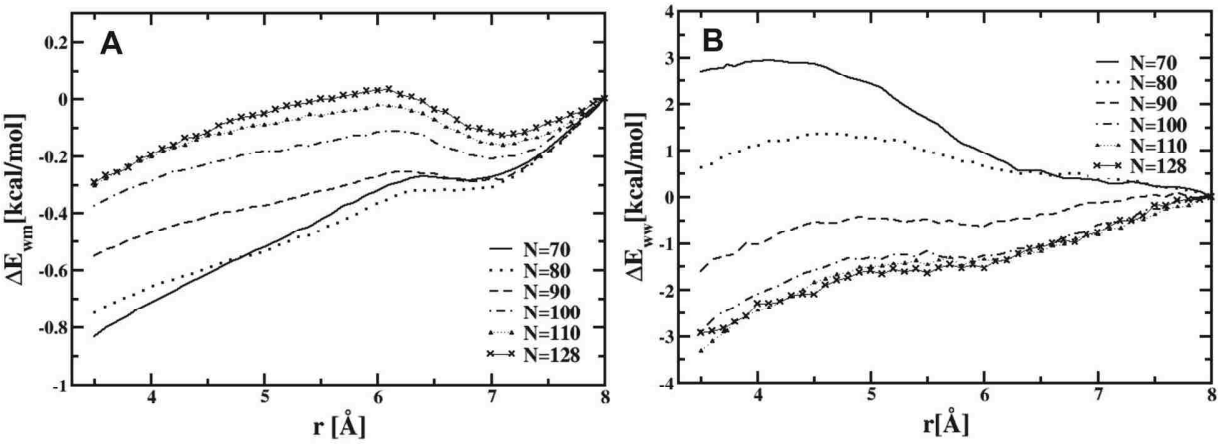

Figure 4.8. Evolution of (**A**) the difference of water-methane interaction energy, ΔE_{wm}, and (**B**) the difference of water-water interaction energy, ΔE_{ww}, as a function of methane pair separation distance, r, from 70 to 128 water molecules.

As shown in Figure 4.6, in the range of water molecules from 90 to 128, water added into a hard sphere fulfills the outer region of a sphere but not the interior region of the sphere, and the possibility of the existence of water molecules near the boundary seems to be similar for both a

short r and a long r. However, the role of the water molecules is different according to the methane pair configurations: For the case of a short r, water molecules continue to complete the second solvation shell resulting in strong water-water interaction energy. For the case of a long r, they continue to complete the first solvation shell for the previously uncovered surface of methane molecules. In addition, due to the location of a methane pair inside a hard sphere, the structure of the second solvation shell at a long r is unsymmetrical and uncompleted. Overall, these different roles of solvent molecules added into a hard sphere result in both stronger water-water interaction energy and less favorable entropy contribution at the CM than at 8.0 Å due to the more complete and ordered second hydration shell for a short r rather than a long r.

4.3.3 General Views on the Evolution of Water Mediated Interactions for a Methane Pair for All Considered Solvent Numbers.

In this section, we address the overview on the evolution of the water mediated interactions including the movement of the positions and their relative stabilities with regard to the CM, BH, and SSM.

Movement of the Positions of the CM, BH, SSM, and 8 Å We tabulated the positions of the CM, BH, and SSM with regard to the number of water molecules added into a hard sphere in Table 4.1. As the number of water molecules increases, the CM shifts into the inwards from 4.2 Å, a minimum position for a bare methane pair used in this study, to 3.8 Å. This observation indicates that a methane pair prefers to move closer to each other as the water density inside a hard cavity increases in order to reduce the surface costs for creating an interface between the hydrophobic molecule and water. On the other hand, the BH started to develop broadly after the addition of 30 water molecules at r of 5.5 Å. The BH then moved to a shorter r until almost half of the water molecules used in this study (approximately 70 number of water molecules, r of 5.2 Å) were added before finally shifting to the outside.

Table 4.1. Positions of CM, BH, and SSM with regards to the solvent number. (NC means "not calculated".)

# of water molecules	*CM (Å)*	*BH (Å)*	*SSM (Å)*
10	4.2	NC	NC
20	4.2	NC	NC
30	4.0	5.5	NC
40	4.0	5.5	NC
50	3.9	5.3	NC
60	3.9	5.2	NC
70	3.8	5.2	NC
80	3.8	5.6	NC
90	3.8	5.6	6.9
100	3.8	5.6	6.8
110	3.8	5.6	6.8
120	3.8	5.6	6.6
128	3.8	5.7	6.4

Table 4.2. Free energy differences obtained from $F_{BH} - F_{CM}$, $F_{BH} - F_{SSM}$, $F_{BH} - F_{8Å}$, $F_{SSM} - F_{CM}$, and $F_{8Å} - F_{CM}$ with regard to the solvent number. (NC means "not calculated". Uncertainties for all obtained values of free energy differences are less than $\pm 4.0 \times 10^{-2}$ kcal/mol.)

# of water molecules	$F_{BH} - F_{CM}$ *(kcal/mol)*	$F_{BH} - F_{SSM}$ *(kcal/mol)*	$F_{BH} - F_{8Å}$ *(kcal/mol)*	$F_{SSM} - F_{CM}$ *(kcal/mol)*	$F_{8Å} - F_{CM}$ *(kcal/mol)*
10	NC	NC	NC	NC	0.24
20	NC	NC	NC	NC	-0.15
30	0.26	NC	0.80	NC	-0.53
40	0.41	NC	1.31	NC	-0.89
50	0.52	NC	1.76	NC	-1.24
60	0.49	NC	1.72	NC	-1.23
70	0.75	NC	1.36	NC	-0.60
80	1.07	NC	0.77	NC	0.30
90	1.27	0.28	0.24	0.99	1.03
100	1.40	0.21	-0.02	1.19	1.43
110	1.48	0.19	-0.13	1.29	1.61
120	1.45	0.15	-0.25	1.29	1.69
128	1.36	0.08	-0.43	1.28	1.78

Relative Stabilities of the CM, BH, SSM, and 8 Å Table 4.2 shows the free energy differences between two different methane pair configurations among the CM, BH, SSM, and 8 Å with regard to the solvent number, N. This table shows, by gradual addition of solvent

molecules into a hard sphere, that generally the free energy difference between the BH and the CM (or Dissociation Barrier Height (DBH)) obtained from F_{BH}-F_{CM} increases, while the free energy difference between the BH and the SSM (or called Association Barrier Height (ABH)) obtained from F_{BH}-F_{SSM} decreases. The obtained values in Table 4.2 indicate that the association tendency of two nonpolar molecules becomes more favorable while dissociation becomes less favorable as water density inside a hard sphere increases.

One question that arose during the water molecule addition events is whether we can observe the bulk-like hydrophobic interaction for a methane pair at a certain density range of water molecules inside a sphere. It has been reported that, generally, the DBH and ABH for a methane pair are around 0.8 ~ 1.0 kcal/mol and 0.3 ~ 0.4 kcal/mol in the bulk.[3-6] Although the DBH is similar to that in the bulk when observed from 70 to 80 water molecules, the SSM has not yet developed in this range of water molecules. Over the entire range of water molecules studied here, we cannot observe bulk-like hydrophobic interaction behaviors for a methane pair during the addition event of water molecules.

4.4 Conclusions.

We have investigated water mediated interactions for a small hydrophobic solute pair with respect to their separation distance and the solvent number. The gradual adding water molecules with this pair involved the addition of 10 to 128 molecules inside a hard sphere of a diameter of 20 Å with a fixed methane pair separated at a certain distance from 3.5 to 8 Å. As expected, microsolvation behaviors for a methane pair configuration are different due to the positions of the two methane molecules inside a hard sphere. Further, this solvation dependence on methane pair configurations inside a hard sphere plays an important role in determining hydration thermodynamics (i.e., PMF and the contributions of both entropy and energy to this PMF). We have shown the relevance for the evolution of hydration thermodynamics to the different

microsolvation behaviors for a methane pair inside a cavity by choosing a methane pair separation of 3.8 Å as being representative of a short r and 8.0 Å as being representative of a long r.

A major difference between the two different methane pair configurations is the accessibility of the space between the two methane molecules for a short r and a long r. In the case of a short r, there is not enough space between the two methane molecules for water molecules to enter, thus the pair functions like one big hydrophobic solute molecule. On the other hand, in the case of a long r, water can access the space between the two methane molecules, leading to the formation of a water network across the center of a hard sphere.

After a hard sphere has been filled with 80 water molecules, the first solvation shell of the two methane molecules (at a short r) is almost completely formed, and the PMF at a short r has become more unfavorable than the PMF at a long r. For a short r, the water molecules added at the beginning are filling mostly half of a hard sphere while simultaneously solvating the surface of two methane molecules at contact. In this case, water molecules located near the boundary of a hard sphere have more broken hydrogen bonds which lead to both unfavorable water-water interaction energies and favorable entropy contributions. These relatively unfavorable water-water interaction energies and favorable entropy contributions reach their maximum around 60 water molecules, which is approximately half of the water molecules used in this study. On the other hand, due to the accessibility of the space between two methane molecules for a long r, water added into a hard sphere can fulfill the inside making a stronger water-water network. This behavior results in more favorable water-water interaction energy and a less favorable entropy contribution than for a short r. In the range of water molecules from 90 to 128, water added into a hard sphere fulfills the outer region of a sphere, and the possibility of the existence of water molecules near the boundary seems to be similar for both a short r and a long r. For a short r,

water molecules continue to complete the second solvation shell resulting in strong water-water interaction energy. For a long r, on the other hand, they continue to complete the first solvation shell for the uncovered surface of methane molecules. In addition, due to the location of a methane pair inside a hard sphere, the structure of the second solvation shell at a long r is unsymmetrical and uncompleted leading to less favorable water-water interaction energy than a short r.

4.5 References.

(1) Keasler, S. J.; Nellas, R. B.; Chen, B., Water mediated attraction between repulsive ions: a cluster-based simulation approach, *J. Chem. Phys.* **2006**, *125*, 144520.

(2) Masunov, A.; Lazaridis, T., Potentials of mean force between ionizable amino acid side chains in water, *J. Am. Chem. Soc.* **2003**, *125*, 1722-1730.

(3) Smith, D. E.; Haymet, A. D. J.; David E. Smith, A. D. J. H., Free energy, entropy, and internal energy of hydrophobic interactions: Computer simulations, *J. Chem. Phys.* **1993**, *98*, 6445-6454.

(4) Smith, D. E.; Zhang, L.; Haymet, A. D. J., Entropy of association of methane in water: a new molecular dynamics computer simulation, *J. Am. Chem. Soc.* **1992**, *114*, 5875-5876.

(5) Dang, L. X., Potential of mean force for the methane-methane pair in water, *J. Chem. Phys.* **1994**, *100*, 9032-9034.

(6) Lüdemann, S.; Schreiber, H.; Abseher, R.; Steinhauser, O., The influence of temperature on pairwise hydrophobic interactions of methane-like particles: A molecular dynamics study of free energy, *J. Chem. Phys.* **1996**, *104*, 286.

CHAPTER 5 THERMODYNAMICS OF WATER FILLING OF A SLIT-LIKE PORE OBSERVED BY NUCLEATION BASED COMPUTER SIMULATION.

5.1 Introduction.

Water plays a critical role in living systems and most terrestrial chemical reactions. Given its importance, water has been the subject of more scientific research than virtually any other system. In particular, an understanding of water phase behavior in non-bulk systems has received great attention due to its biological, technological, and atmospheric importance.

One of the most important environments affecting water phase behavior is confinement. Water clusters confined in nanoscale geometries are common in biology, engineering and geology. Confinement can significantly alter the water structure, producing phase behavior that is quite distinct from both bulk water and clusters not under confinement.[1, 2 3]In addition, these alterations to the water structure can significantly modify its interactions with solute molecules. For example, in a solvent driven process such as protein folding, perturbing the solvent structure by confinement can induce considerably different kinetic and thermodynamic properties to the protein folding process compared to those observed in bulk phases.[4-7] In particular, the collapse of biopolymers leading to the formation of a water expelling nonpolar cavity is believed to be the central theory for the protein folding process and its stability.[8] However, conflicting results have been reported about whether the interior of the hydrophobic cavity that is formed is actually 'empty' or 'wet'.[8-11] Some researchers have reported that buried water inside the protein structure is required, at least transiently, in nonpolar cavities for their functions. In addition, this interior hydration of proteins has also been suggested as a mechanism of pressure induced protein unfolding.

Most researches have paid much attention to the hydration thermodynamics of nonpolar solute molecules in aqueous solutions and the water induced hydrophobic interactions.

Conversely, the behavior of water molecules in non-aqueous solutions or environments has been relatively less studied. In this chapter, we will analyze the interior hydration thermodynamics by adding water molecules in between two smooth parallel walls using our nucleation technique, AVUS-HR.[12, 13] We have also addressed the effects of dimensionality, as well as the interaction between water molecules and walls, on such hydration thermodynamics.

5.2 Simulation Methods.

Our grand canonical version of the vapor-liquid nucleation algorithm has been applied to the extension of studies on hydration thermodynamics of water molecules in nonpolar cavities. We have restricted the formation of water droplets to inside the cavities only, otherwise rejecting any trial moves that intend to place a water molecule outside. As a model of hydrophobic cavities, we used two infinite smooth walls, as shown in Figure 5.1, and restricted the movement of water molecules along the z-directions again by rejecting any trial moves that exceed the boundary. We used periodic boundary conditions for the x and y directions with a gradual addition of water molecules between the walls. As part of the simulation conditions, the chemical potential of the gas-phase was specified and the interaction between this gas phase and the water molecules was neglected here.

The TIP4P[14] interaction parameter was used for water-water interactions, and the energy-based Stillger-type cluster criterion[15, 16] was used for the cluster criterion. We set -260K as the water cluster criterion based on our previous water vapor-liquid nucleation studies.[12, 17] For the interaction parameters between water molecules and walls, we used ideal hydrophobic walls, also termed hard walls, which excludes water molecules from a certain region in space and for which there is no interaction between the water and the walls. Moreover, in order to address the effects of water-wall interaction, we added weak attractive interaction parameters between them.

The 9-3 type potential, which is appropriate for a homogeneous solid surface,[18] is used for water-wall interaction potential type and is depicted by Equation 5-1 below:

$$U(\Delta z) = 4\varepsilon_{ow}\left[\left(\frac{\sigma_{ow}}{\Delta z}\right)^9 - \left(\frac{\sigma_{ow}}{\Delta z}\right)^3\right] \qquad 5\text{-}1$$

In this equation, ΔZ is the distance from the oxygen atom of a water molecule to the hydrophobic walls, whereas ε_{ow} and σ_{ow} refer to the interaction parameters between the oxygen atom of a water molecule and a hydrophobic wall. We set ε_{ow} = 1.237 kJ/mol and σ_{ow} = 2.4735 Å. These parameters were chosen to mimic the interaction of a water molecule with the paraffin-like wall.[19, 20] For this type of wall, the effective wall separation, H_{eff}, can be used to define the region accessible to the water molecules added into the inter plate region. H_{eff} was defined to be the distance between points at which the potential energy, $U(\Delta z)$**,** is zero: These points are located at $-Z_0 + 2.4735$Å and $Z_0 - 2.4735$Å where $\pm Z_0$ are the positions of the origins of the walls. All pair Lennard Jones and electrostatic interactions were also considered during the simulations.

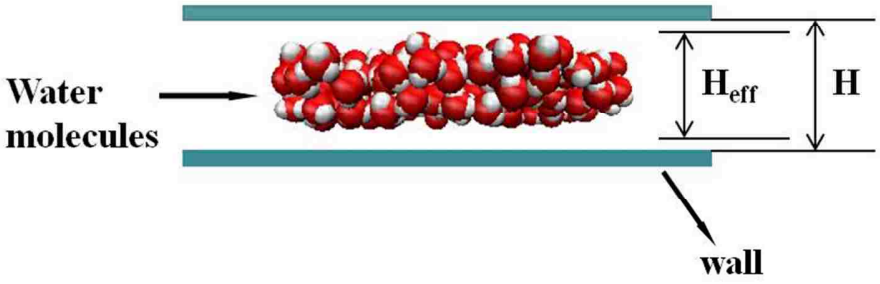

Figure 5.1. Schematic of the simulated confined water systems between two smooth parallel walls in an xy plane, separated by H. This figure also includes the effective wall separation, H_{eff}. In the case for hard walls, H equals to H_{eff}.

5.3 Results and Discussion.

Before starting this results section, we would like to note that we compared resulting thermodynamic properties for hard walls with those for paraffin-like walls based on the

assumption that the effective wall-wall separation, H_{eff}, for hard walls is equal to the wall-wall separation, H.

5.3.1 Free Energy Penalty during Water Filling Process of Wall-Wall Interspace.

How much free energy penalty is required for adding water molecules into the confining space between two parallel walls? In order to address this question, we calculated the free energy difference between two states of confining systems using the following equation:

$$\Delta\Delta G_{H_{eff}}(N) = \Delta G_{H_{eff}}(N) - \Delta G_{\inf inite}(N) \qquad 5\text{-}2$$

In this equation, $\Delta\Delta G_{Heff}(N)$ is the free energy difference between $\Delta G_{Heff}(N)$, which is the nucleation free energy for forming water droplets of size N in a confining space between two parallel walls with a wall-wall separation of H_{eff}. The term $\Delta G_{infinite}(N)$ represents the nucleation free energy for forming water droplets of size N in a confining space between two parallel walls with an infinite wall-wall separation. For the case of a hard wall, where there is no interaction between water molecules and the wall, this free energy penalty for a certain wall-wall separation, H_{eff}, is equal to the work required for the process of bringing two parallel hard walls from far apart (or infinite wall-wall separation where there is no correlation between the position of the two parallel walls) to a certain wall-wall distance, H_{eff}. This required work is equal to the water induced PMF. Therefore, similar to the PMF calculation for small hydrophobic solute molecules, the water induced PMF of hard walls for the number of water molecules as a function of wall-wall separation distance is calculated by the following steps:

1) Run the simulation of the vapor liquid nucleation method called AVUS-HR for a certain wall-wall separation, H_{eff}, by gradually adding water molecules into interspace between two parallel hard walls.

2) With the obtained association free energy (or nucleation free energy) for a certain wall–wall separation of H_{eff}, $\Delta G_{Heff}(N)$, the association free energy difference between two different wall-wall separations can be calculated through the thermodynamic cycles depicted in Figure 2.3.

Initially, we displayed the free energy penalty of hard walls for the number of water molecules (N) as a function of the wall-wall separation, H_{eff}, in Figure 5.2. As expected, the free energy penalty for the water filling process into the confining space between two hard walls increases as N increases for each wall-wall separation. In addition, the extent of this free energy increased amount becomes smaller as the wall-wall separation becomes larger from 3 Å to 10 Å.

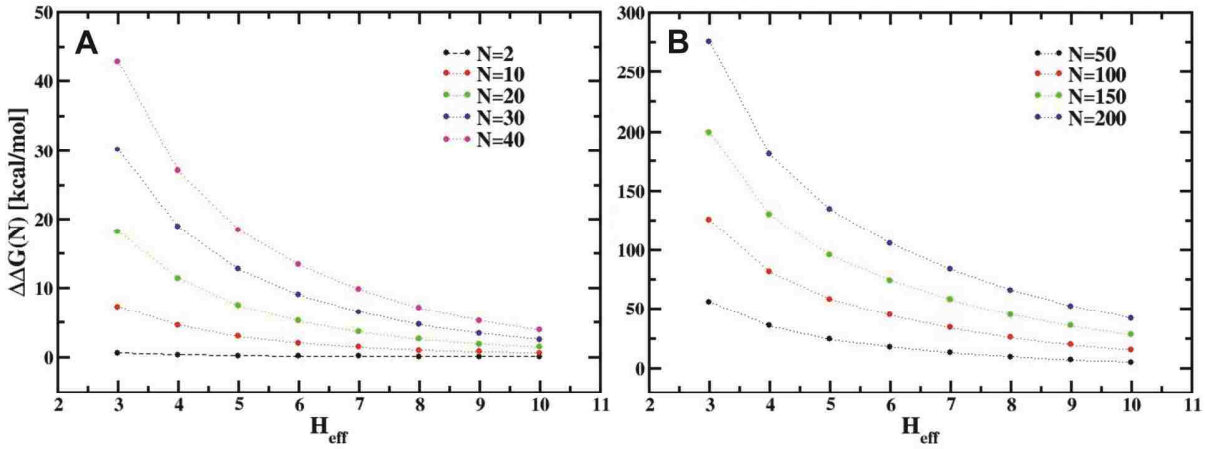

Figure 5.2. Free energy penalty (or water induced PMF) of hard walls for the different number of water molecules (N) as a function of wall-wall separation (H_{eff}). The units for $\Delta\Delta G(N)$ are kcal/mol.

Is this water filling process in confinement between two paraffin-like walls favorable or unfavorable? In order to determine how the presence of weak attractive interactions between water molecules and walls affects the water filling process, we also calculated the free energy penalty for paraffin-like walls in Figure 5.3. This data suggests that weak attractive interaction between water molecules and walls allows the initial filling process to be much easier than in the hard wall case (i.e. no interaction between the water and the wall) and even better than the infinite wall-wall separation case.

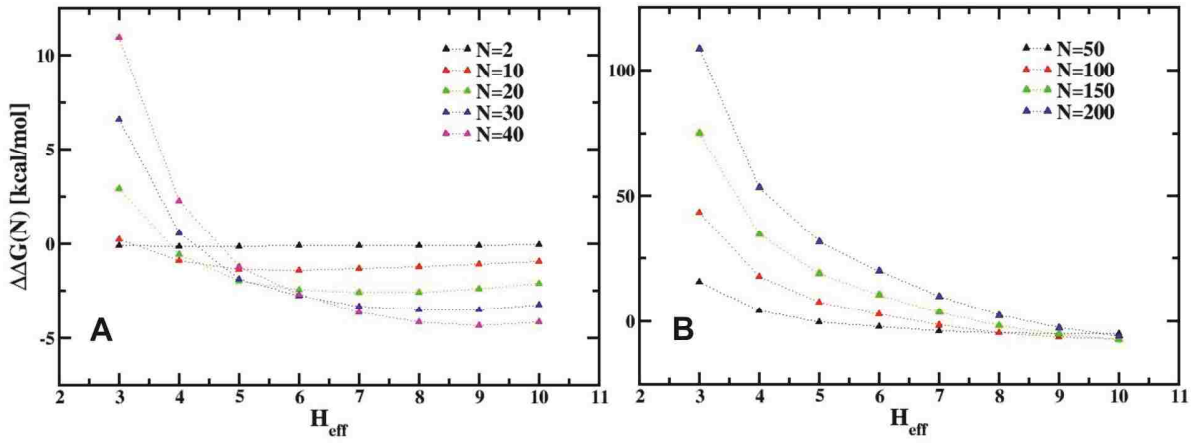

Figure 5.3. Free energy penalties of paraffin-like walls for the number of water molecules (N) as a function of wall-wall separation (H_{eff}). The units of $\Delta\Delta G(N)$ are kcal/mol.

Interesting features for paraffin-like walls are observed in Figure 5.3: Initial addition of water molecule is slightly more favorable than for the infinite wall-wall separation case. When adding 10 water molecules, the free energy penalty for H_{eff} at 3 Å starts to become positive (or unfavorable) while free energy penalties for other wall-wall separations continue to be negative. When adding 10 more water molecules (N=20), the free energy penalty for H_{eff} at 4 Å becomes less negative and so on. The number of water molecules, N, where the free energy penalty starts to be less negative increases as the H_{eff} are getting larger. The reason for this behavior of the free energy penalty may be considered as the result of a competition between favorable water-wall interaction energy and unfavorable water-water interaction energy from restricted space when adding water molecules. In the following section, we will further discuss the behavior of differences of water-water and water-wall (for paraffin-like wall case) interaction energy as a function of H_{eff} and N.

5.3.2 Roles of Water-Water Interaction Energy and Water-Wall Interaction Energy.

The difference of the water-water interaction term, ΔE_{ww}, and the difference of water-wall interaction term, $\Delta E_{water\text{-}wall}$, were obtained from direct calculations during the simulations.

Generally, the water-water interaction energy is not more favorable for water clusters of any size formed in a confining space between two hard walls than in an infinite wall-wall separation (Figure 5.4). This tendency of unfavorable water-water interaction energy increases both as H_{eff} decreases and as the water cluster size increases. A characteristic feature for a hard wall is that H_{eff} at 3 Å has a distinctive unfavorable water-water interaction energy than at other separation distances. This feature can be attributed to a very small space (near to 2 dimensions) where only one strand of water molecule can be adopted. Thus, unfavorable water-water interaction energy is alleviated when H_{eff} increases to some extent where two or more strands of water molecules can exist inside the confining space leading to a more flexible formation of the water-water network.

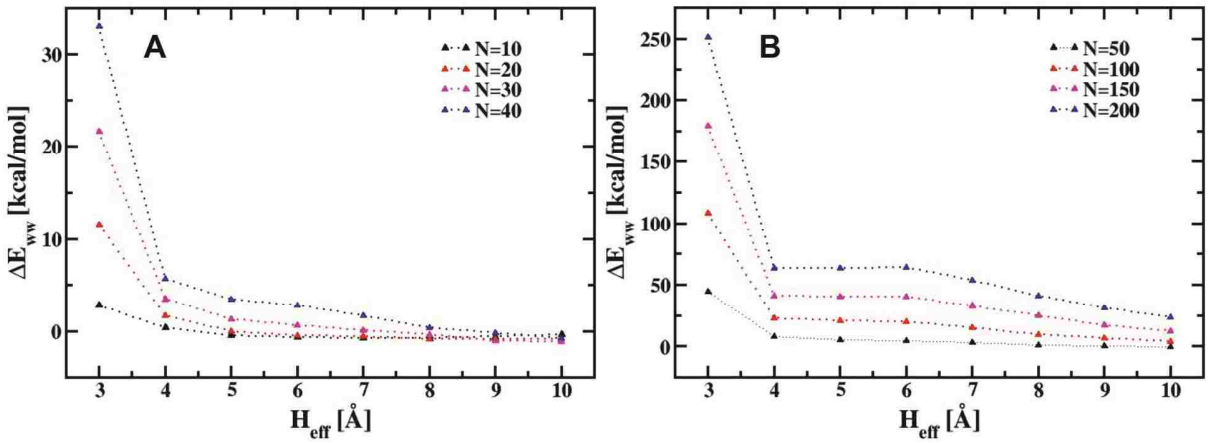

Figure 5.4. The difference of the water-water interaction energy, ΔE_{ww}, of hard walls as a function of wall-wall separation distance, H_{eff}. We set the infinite wall-wall separation as the reference.

The existence of weak attractive interactions between water molecules and walls generally makes the unfavorable water-water interaction decrease by allowing a more flexible water orientation for formation of a water network. This observation is in contrast to hard wall cases, although the size of the confining space for entering water molecules is the same between the two different types of walls (i.e., hard walls and paraffin-like walls). For example, for the case of

H_{eff} at 3 Å, transverse water density profiles show that water molecules can form two complete strands of water molecules for a paraffin-like wall while only one strand of water molecules forms for a hard wall. We also evaluated the interaction between water molecules and walls, $\Delta E_{water\text{-}wall}$, and displayed the difference of total energy for a water cluster system, ΔE_{total}, by summing ΔE_{ww} and $\Delta E_{water\text{-}wall}$ (Figure 5.5). The water-wall interactions become more attractive as H_{eff} decreases while N increases. These negative values result in a lowering of the total energy of the system.

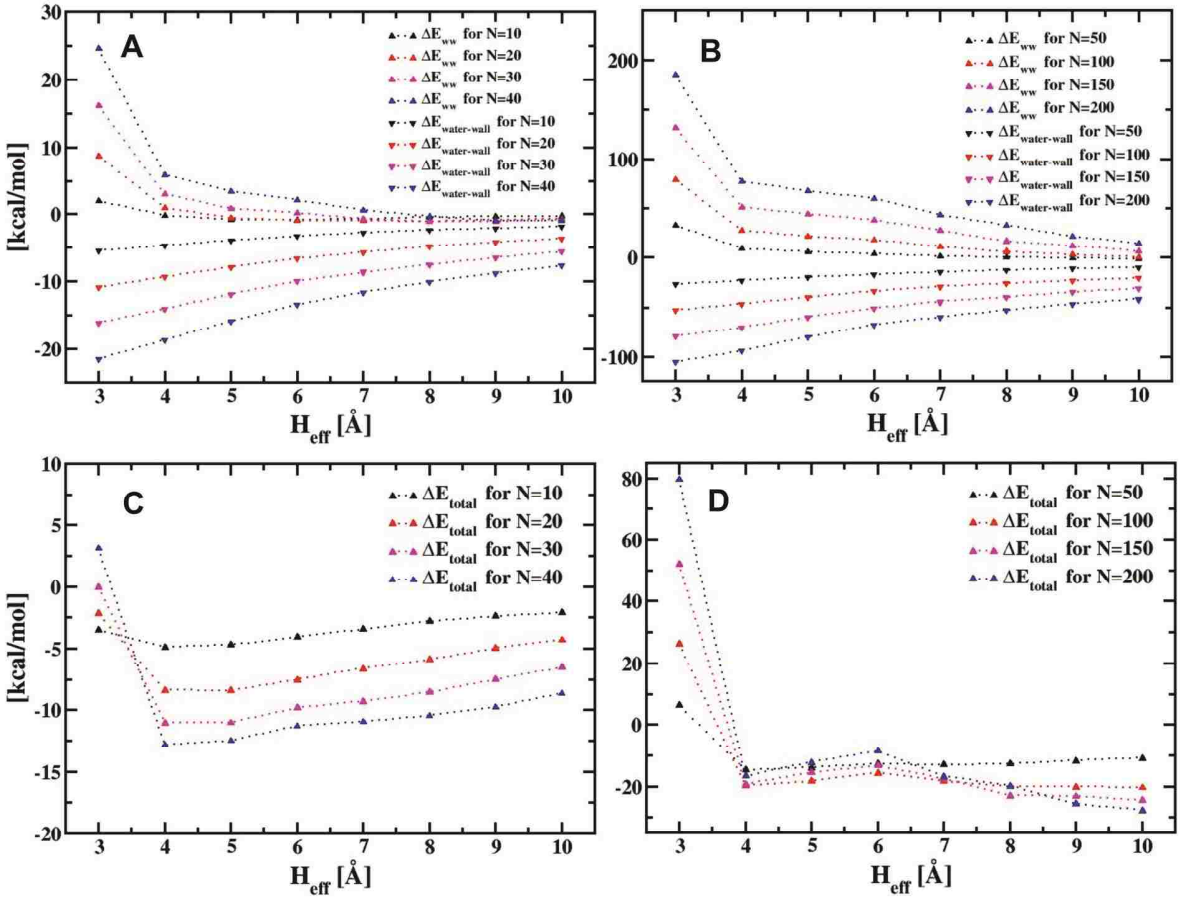

Figure 5.5. The difference of the water-water interaction energy, ΔE_{ww}, and the water-wall interaction energy, $\Delta E_{water\text{-}wall}$, of paraffin-like walls as a function of wall-wall separation distance, H_{eff}. The difference of total energy of the system, ΔE_{total}, for a paraffin-like wall is also included in this figure. We set infinite wall-wall separation as the reference.

5.3.3 Oxygen Number Density Profiles.

It is well known that water layering is induced when water molecules are placed in two or three molecular diameter-size confined environments in order to pack themselves, regardless of the water-wall interaction.[21-24] Generally, this layering can be shown as the transverse density profiles of water molecules along the direction perpendicular to the wall. This transverse density profile can be considered as the two body pair correlation function displaying radial density of the water oxygen molecules with regard to the wall, which is fixed in space with an infinite curvature. Further, both the magnitude and the water layering structure depend on the density of water molecules and the water-wall interaction.

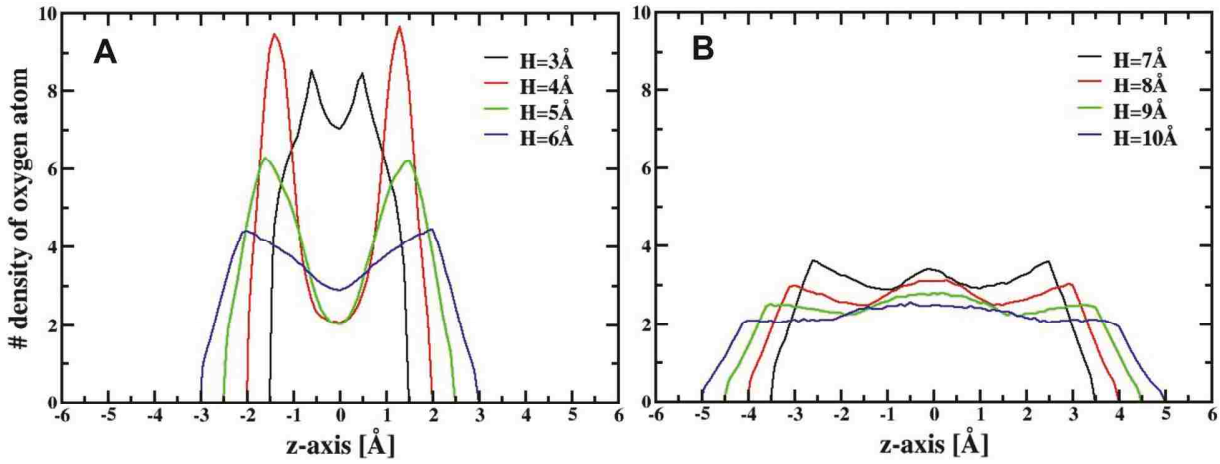

Figure 5.6. Oxygen number density profiles along the confinement direction, z-axis, for different wall separations of (**A**) 3, 4, 5, 6 and (**B**) 7, 8, 9, 10 Å for hard walls.

We analyzed the oxygen number density profiles by computing the average number of water oxygen atoms in slabs of a specific thickness (Δz = 0.1 Å) along the direction perpendicular to the wall (central plane at z= 0) for hard walls in Figure 5.6. When H_{eff} = 3 Å, water is under transition from one layer to two layers, depicted graphically by having two small peaks. When H_{eff} = 4 Å, the water has formed two layers shown by two sharp peaks near each wall. These two layers of water are getting broader as H_{eff} increases from 4 to 6 Å. Finally, three water layers

were formed at H_{eff} = 7 Å having a broad peak in the middle of a confining slab between two hard walls. This formed three layers continues to be broader until H_{eff} = 10 Å.

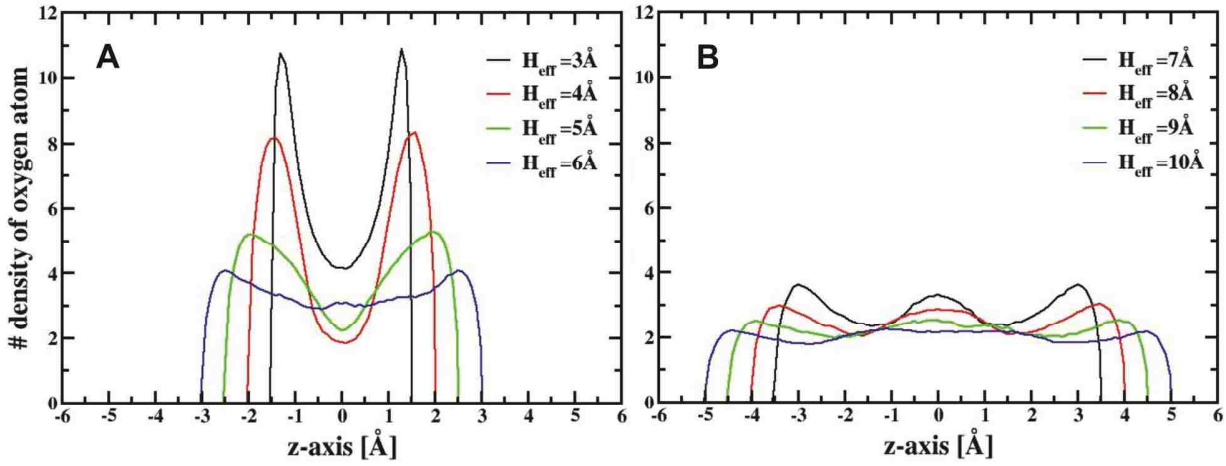

Figure 5.7. Oxygen number density profiles along the confinement direction, z-axis, for different wall separations of (**A**) 3, 4, 5, 6 and (**B**) 7, 8, 9, 10 Å for paraffin-like walls.

In order to show the effect of weak attractive interactions between the water and the wall on water packing behavior, we also performed the same transverse density analysis for paraffin-like walls. As shown in Figure 5.7, the notable observed difference is in the water packing behavior at H_{eff} = 3 Å: While water is under transition between one to two layers for hard wall case, water initially forms two layers for paraffin-like walls due to the weak attractive interaction between the water and the wall. Although general water layering behavior after H_{eff} = 3 Å is similar to the layering behavior for hard walls, the height of the two peaks near each wall, for a paraffin-like wall, is taller than the height for a hard wall at H_{eff} = 4,5 and 6 Å. Another interesting difference between hard and paraffin-like walls is that the summit of the peaks for a paraffin-like wall is broader than those for a hard wall, which may also result from the weak attractive interaction between the water and the wall.

From the transverse water density profiles for hard and paraffin-like walls, it is obvious that the water-wall interaction affects the way water is packed into a confining space. However, this

paraffin-like wall does not provide a significant difference from the hard wall case except for the smallest effective wall separation (3 Å).

5.4 Conclusion.

As an extension of the work for hydrophobic interactions between small hydrophobic solutes in confined environments, we applied a novel nucleation algorithm termed AVUS-HR to the extremely large hydrophobic solute systems such as two infinitely parallel walls. In order to adjust the original nucleation algorithm for analysis of the infinitely parallel wall system, we slightly modified it in such a way that the applied Monte Carlo move is only accepted when it leads to water droplet formation inside the confined environment made by the two walls, otherwise the trial move is rejected. To address the effects of water-wall interaction on the behaviors of confined water, the weak attractive interaction between water molecules and walls are added for comparison to the hard wall case.

The simulation result reveals that the weak attractive interaction between water molecules and walls allows water molecules to pack more efficiently for making water networks. Thus, these weak interactions lower the free energy penalty for the formation of water clusters in a confined space between two walls, ultimately lowering the total energy of the system when compared with the hard wall case (where there is no interaction between water molecules and walls).

Through the work described in this chapter, we show the successful application of our nucleation algorithm to the study of the properties of water molecules (i.e., both qualitative properties such as water layering behavior and quantitative properties such as free energy penalty and water-water interaction terms) confined between two large hydrophobic solutes expressed as infinitely parallel walls.

In conclusion, we have successfully applied our novel nucleation algorithm to two different hydrophobicity-related simulation studies, one on hydrophobic association behavior between two small hydrophobic solute molecules under confined environment and the other on hydration thermodynamics under confined space between two infinitely parallel walls. This information will further our understanding of the various and more complex hydrophobic phenomena (i.e., association behaviors of nonpolar and/or polar amino acid residues under confined environment, and effects of salts, temperature and pressure on this association behaviors) as well as nucleation events under confined environment.

5.5 References

(1) Zangi, R.; Mark, A. E., Monolayer ice, *Phys. Rev. Lett.* **2003**, *91*, 025502.

(2) Koga, K.; Gao, G. T.; Tanaka, H.; Zeng, X. C., Formation of ordered ice nanotubes inside carbon nanotubes, *Nature* **2001**, *412*, 802-805.

(3) Giovambattista, N.; Rossky, P.; Debenedetti, P., Phase Transitions Induced by Nanoconfinement in Liquid Water, *Phys.Rev. Lett.* **2009**, *102*.

(4) Zhou, H. X., Protein folding and binding in confined spaces and in crowded solutions, *J. Mol. Recognit.* **2004**, *17*, 368-375.

(5) Rathore, N.; Knotts, T. A. t.; de Pablo, J. J., Confinement effects on the thermodynamics of protein folding: Monte Carlo simulations, *Biophys. J.* **2006**, *90*, 1767-1773.

(6) Eggers, D. K.; Valentine, J. S., Molecular confinement influences protein structure and enhances thermal protein stability, *Protein Sci.* **2001**, *10*, 250-261.

(7) Zhou, H. X.; Rivas, G.; Minton, A. P., Macromolecular crowding and confinement: biochemical, biophysical, and potential physiological consequences, *Annu. Rev. Biophys.* **2008**, *37*, 375-397.

(8) ten Wolde, P. R.; Chandler, D., Drying-induced hydrophobic polymer collapse, *Proc. Natl. Acad. Sci. USA* **2002**, *99*, 6539-6543.

(9) Shea, J. E.; Onuchic, J. N.; Brooks, C. L., 3rd, Probing the folding free energy landscape of the Src-SH3 protein domain, *Proc. Natl. Acad. Sci. USA* **2002**, *99*, 16064-16068.

(10) Cheung, M. S.; García, A. E.; Onuchic, J. N., Protein folding mediated by solvation: water expulsion and formation of the hydrophobic core occur after the structural collapse, *Proc. Natl. Acad. Sci. USA* **2002**, *99*, 685-690.

(11) Liu, P.; Huang, X.; Zhou, R.; Berne, B. J., Observation of a dewetting transition in the collapse of the melittin tetramer, *Nature* **2005**, *437*, 159-162.

(12) Chen, B.; Siepmann, J. I.; Klein, M. L., Simulating vapor-liquid nucleation of water: A combined histogram-reweighting and aggregation-volume-bias Monte Carlo investigation for fixed-charge and polarizable models, *J. Phys. Chem. A* **2005**, *109*, 1137-1145.

(13) Nellas, R. B.; McKenzie, M. E.; Chen, B., Probing the nucleation mechanism for the binary n-nonane/1-alcohol series with atomistic simulations, *J. Phys. Chem. B* **2006**, *110*, 18619-18628.

(14) Jorgensen, W. L., Quantum and statistical mechanical studies of liquids. 10. Transferable intermolecular potential functions for water, alcohols, and ethers. Application to liquid water, *J. Am. Chem. Soc.* **1981**, *103*, 335-340.

(15) Chen, B.; Siepmann, J. I.; Oh, K. J.; Klein, M. L., Aggregation-volume-bias Monte Carlo simulations of vapor-liquid nucleation barriers for Lennard-Jonesium, *J. Chem. Phys.* **2001**, *115*, 10903-10913.

(16) Chen, B.; Siepmann, J. I.; Oh, K. J.; Klein, M. L., Simulating vapor-liquid nucleation n-alkanes, *J. Chem. Phys.* **2002**, *116*, 4317-4329.

(17) Keasler, S. J.; Nellas, R. B.; Chen, B., Water mediated attraction between repulsive ions: a cluster-based simulation approach, *J. Chem. Phys.* **2006**, *125*, 144520.

(18) Allen, M. P.; Tildesley, D. J. *Computer simulation of liquids*; Oxfold science press, 1989.

(19) Lee, C. Y.; McCammon, J. A.; Rossky, P. J., structure liquid water extended hydrophobic surface, *J. Chem. Phys.* **1984**, *80*, 4448-4455.

(20) Kumar, P.; Buldyrev, S. V.; Starr, F. W.; Giovambattista, N.; Stanley, H. E., Thermodynamics, structure, and dynamics of water confined between hydrophobic plates, *Phys. Rev. E* **2005**, *72*, 051503.

(21) Hua, L.; Zangi, R.; Berne, B. J., Hydrophobic Interactions and Dewetting between Plates with Hydrophobic and Hydrophilic Domains, *J. Phys. Chem. C* **2009**, *113*, 5244-5253.

(22) Giovambattista, N.; Debenedetti, P. G.; Rossky, P. J., Hydration Behavior under Confinement by Nanoscale Surfaces with Patterned Hydrophobicity and Hydrophilicity, *J. Chem. Phys. C* **2007**, *111*, 1323-1332.

(23) Lee, S. H.; Rossky, P. J., A comparison of the structure and dynamics of liquid water at hydrophobic and hydrophilic surfaces—a molecular dynamics simulation study, *J. Chem. Phys.* **1994**, *100*, 3334.

(24) Zangi, R., Water confined to a slab geometry: a review of recent computer simulation studies, *J. Phys.-Condens. Mat.* **2004**, *16*, 0-S5388.

VITA

Hyunmi Kim was born in Changnyeong, Korea, on May 24th, 1979. She received her Bachelor of Science degree in Chemistry from Chung-Ang University, Seoul, Korea, in February of 2002. Under the supervisor of Professor Jin-ho Choy, she built her research experience at National Nanohybrid lab in the Department of Chemistry at Seoul National University, Seoul, Korea. In February of 2004, she acquired her Master of Science in Chemistry with the thesis: "Studies on Inorganic-Drug Nanohybrid as Drug Delivery System; Laponite-Itraconazole" She began her graduate studies in the Department of Chemistry at Louisiana State University, Baton Rouge, Louisiana in August of 2006, and will receive her Doctor of Philosophy in computational chemistry in December of 2011 with the thesis: "A Multifaceted Phenomenon of Hydrophobic Effects: Insights Learned from Nucleation Algorithm based Computer Simulation Approach".